Finite-State Uncertainty-Aware Widely-Linear Equalization for Aeronautical GMSK Links

Ahmad Tanha, *Member, IEEE* and Ali Khalesi, *Member, IEEE*

arXiv:2610.38638v1 [eess.SP] 28 Oct 2026

***Abstract*—Aeronautical and unmanned aerial vehicle (UAV) receivers must equalize doubly selective channels under synchronization uncertainty and limited onboard computation and memory. We propose a finite-state, uncertainty-aware widely-linear (WL) equalization algorithm for Gaussian minimum-shift keying (GMSK) links. The algorithm uses synchronization estimates and their reliability descriptors to select one of a small number of precomputed filters, avoiding repeated online coefficient synthesis. Using a finite-memory Laurent model, we design the stored affine WL filters from conditional physical-state moments. We derive an exact characterization of excess mean-square error (MSE) relative to adaptation to continuous side information, Lloyd-type conditions for finite-state design, local timing–frequency mismatch certificates, and an orthogonal decomposition of design and information losses. On a reference channel at $E_b/N_0 = 8$ dB under high synchronization-estimation uncertainty, a 16-state bank reduces pseudo-symbol MSE by 51.9% relative to point-estimate WL time-varying MMSE equalization and by 6.6% relative to posterior-mean (PM) substitution. With identical partitioning, routing, and storage, conditional-moment filters reduce MSE by 10.1% and full-waveform average bit error rate (ABER) by 15.6% relative to representative-state filters. Across 18 synthetic three-path channels with individually fitted banks, MSE and ABER decrease by 5.3% and 12.9%, respectively, relative to PM substitution. The 16-state receiver stores 2048 real coefficients. Posterior integration, robustness sweeps, and software timing measurements quantify the tradeoff between equalization accuracy, online computational cost, and bank refresh.**

***Index Terms*—Aeronautical communications, GMSK, widely-linear equalization, synchronization uncertainty, doubly selective channels, MMSE estimation, finite-state receivers.**

I. Introduction

Aeronautical communication links, including unmanned aerial vehicle (UAV) control and non-payload links, require robust receivers with limited onboard computation and memory [1]. Relative motion and multipath produce doubly selective channels, while imperfect front-end estimation leaves residual timing and frequency uncertainty. Repeated equalizer coefficient synthesis can impose appreciable online cost. We therefore focus on sampled linear and widely-linear (WL) equalizers and propose a finite-state implementation that uses synchronization estimates and reliability information to select uncertainty-aware filters from a precomputed bank.

Gaussian minimum-shift keying (GMSK) has a constant envelope and admits a Laurent continuous-phase modulation (CPM) representation [2], [3]. The resulting pseudo-symbols can be improper, motivating WL processing [4]–[6]. Conjugate observations allow WL processing to exploit these statistics within an affine filtering architecture. Recent work includes WL minimum mean-square error (MMSE) receivers for rectilinear and quasi-rectilinear signals [7], low-complexity WL equalizers for spectrally shaped discrete Fourier transform-spread orthogonal frequency-division multiplexing [8], and satellite-impairment compensation [9]. We focus on uncertainty-aware adaptation under a finite storage budget.

The closest application-specific work develops linear time-varying (LTV) and widely-linear time-varying (WLTV) zero-forcing and MMSE equalizers for CPM over doubly selective UAV links [1]. Our point-estimate plug-in (PI) WLTV-MMSE baseline treats the estimated physical state as exact. We instead design stored filters from covariance and complementary-covariance moments conditioned on the estimates and reliability descriptors assigned to each receiver state. This targets conditions in which synchronization uncertainty degrades point-estimate adaptation but side information still supports effective filter selection. The numerical evaluation includes path Doppler and residual timing–frequency mismatch.

Low-complexity CPM equalization has also exploited frequency-domain band structure [10]. Related approaches partition decoder side information using context trees with local linear turbo equalizers and MMSE-related guarantees [11], or cluster reliability information with local adaptive equalizers [12]. Our partition captures physical-state uncertainty, including synchronization and channel parameters. A matched-budget experiment isolates conditional-moment filter-design gains with partition, routing, and storage fixed.

Bayesian equalization can account for channel uncertainty [13], and complex Gaussian-process regres-

The authors are with the Signals, Telecommunications & AI Department at Institut Polytechnique des Sciences Avancées (IPSA), Ivry-sur-Seine, France. Ali Khalesi is also with LINCS lab, Paris, France. Emails: {ahmad.tanha, ali.khalesi}@ipsa.fr.

sion relates Bayesian inference to WL MMSE estimation [14]. Unlike observation quantization [15], our approach leaves the sampled observation unchanged and compresses receiver adaptation. Specifically, we distinguish the physical state $\boldsymbol{\theta} = (\boldsymbol{\epsilon}, \mathbf{h}, \mathbf{R}_n^{\text{true}})$ from the available side information $\mathsf{S} = (\widehat{\boldsymbol{\epsilon}}, \widehat{\mathbf{h}}, \widehat{\mathbf{R}}_n, \boldsymbol{\zeta})$ and use $p(\boldsymbol{\theta} \mid \mathsf{S})$ to compute conditional moments. Building on classical affine-MMSE projection and Lloyd/Linde–Buzo–Gray (LBG) alternation, we develop a finite-state adaptation framework for synchronization uncertainty.

Our main contributions are summarized below.

- We formulate a finite-state affine-WL equalizer under a fixed storage budget. State estimates and reliability descriptors select precomputed filters designed from conditional physical-state moments, avoiding repeated online coefficient synthesis.
- We characterize the exact finite-state MSE penalty relative to adaptation to continuous side information and specialize classical Lloyd/LBG conditions to excess equalization MSE. We distinguish the threshold-based bank evaluated numerically from unrestricted Lloyd optimization.
- We characterize the side-information and oracle affine-WL limits, decompose plug-in degradation into orthogonal design and information losses, and derive local timing–frequency viability certificates for frozen WLTV equalization relative to the corresponding complex-linear receiver.
- We demonstrate an accuracy–computation tradeoff for resource-limited airborne receivers in terms of MSE and full-waveform average bit error rate (ABER). Reference-channel, multi-channel, and matched-budget experiments assess the benefit of conditional-moment filter design. Comparisons with continuous adaptation, robustness tests, and software timings quantify accuracy, online cost, and bank-refresh requirements.

Notation. Bold lowercase and uppercase letters denote vectors and matrices, respectively; $(\cdot)^T$, $(\cdot)^*$, and $(\cdot)^H$ denote transpose, complex conjugation, and Hermitian transpose. The operators $\mathbb{E}[\cdot]$, $\mathrm{Cov}(\cdot)$, $\mathrm{tr}(\cdot)$, and $\|\cdot\|_2$ denote expectation, covariance, trace, and Euclidean norm, respectively. For Hermitian matrices, $\mathbf{A} \succeq \mathbf{B}$ means that $\mathbf{A} - \mathbf{B}$ is positive semidefinite, and $\mathcal{CN}(\boldsymbol{\mu}, \mathbf{R})$ denotes a proper complex Gaussian distribution with mean $\boldsymbol{\mu}$ and covariance $\mathbf{R}$. Underlined variables denote augmented WL vectors; S and O denote side information and oracle information, respectively.

II. System Model and Problem Formulation

We model a doubly selective GMSK link with imperfect front-end information and formulate uncertainty-aware adaptation within the affine widely-linear (WL) receiver class.

A. GMSK Block Representation

Let $\{a_m\}$, $a_m \in \{-1, +1\}$, denote a binary GMSK sequence with symbol duration T. GMSK is a binary CPM with modulation index $h = 1/2$ and Gaussian frequency pulse shaping [2]. Using Laurent's decomposition [3], the adopted finite-memory GMSK waveform over the observation interval can be represented as

$$s(t) = \sum_{k=1}^{K} b_k g_k(t), \tag{1}$$

where k indexes a Laurent component and its time shift, g_k is the corresponding pulse, and b_k is its data- and phase-state-dependent pseudo-symbol. The analysis uses the exact representation of the adopted finite-memory model over the observation interval; dominant-component truncation is used only in the numerical implementation.

We collect the pseudo-symbols as

$$\mathbf{b} = \begin{bmatrix} b_1 & \cdots & b_K \end{bmatrix}^T. \tag{2}$$

We allow $\mathbf{b}$ to have a nonzero mean. Let $\boldsymbol{\mu}_b = \mathbb{E}[\mathbf{b}]$, and define its centered covariance and pseudo-covariance as

$$\mathbf{R}_b = \mathbb{E}\big[(\mathbf{b} - \boldsymbol{\mu}_b)(\mathbf{b} - \boldsymbol{\mu}_b)^H\big], \tag{3}$$

$$\mathbf{C}_b = \mathbb{E}\big[(\mathbf{b} - \boldsymbol{\mu}_b)(\mathbf{b} - \boldsymbol{\mu}_b)^T\big]. \tag{4}$$

Depending on the pseudo-symbol statistics and phase initialization, $\mathbf{C}_b$ may be nonzero, motivating WL processing.

B. Aeronautical Channel and Residual Synchronization

The channel has L_h paths with delays λ_ℓ and time-varying coefficients $\alpha_\ell[n]$ [1], [16]. For sampling period T_s and known phase-reference start time t_0, sample n has local time nT_s and phase-reference time $t_0 + nT_s$, $n = 0, \ldots, N-1$. We write

$$\alpha_\ell[n] = \bar{\alpha}_\ell[n] e^{j2\pi\nu_\ell(t_0 + nT_s)}, \tag{5}$$

where ν_ℓ is the path Doppler shift and $\bar{\alpha}_\ell[n]$ captures the remaining gain variation. Imperfect synchronization leaves a residual timing error $\Delta\tau$ and a common frequency offset Δf. Unlike path-dependent Doppler, Δf produces the same phase rotation on all paths.

We normalize the residual synchronization errors as

$$\epsilon_\tau = \frac{\Delta\tau}{T}, \qquad \epsilon_\nu = \Delta f\, T, \qquad \boldsymbol{\epsilon} = \begin{bmatrix} \epsilon_\tau \\ \epsilon_\nu \end{bmatrix}. \tag{6}$$

For receive filter $r(t)$, let $\phi_k = g_k * r$ denote the nominal effective Laurent pulse. We adopt a sampled-equivalent phase model in which path Doppler and residual frequency offset act as phase rotations at the sampling instants. Channel phases use $t_0 + nT_s$, while

pulse arguments use local time. The resulting $N \times K$ channel matrix is

$$[\mathbf{H}(\boldsymbol{\epsilon}, \mathbf{h})]_{n,k} = \sum_{\ell=0}^{L_h-1} \bar{\alpha}_\ell[n]\, e^{j2\pi(t_0+nT_s)(\nu_\ell+\epsilon_\nu/T)} \times \phi_k\left(nT_s - \lambda_\ell - T\epsilon_\tau\right), \tag{7}$$

where

$$\mathbf{h} \triangleq \left\{ \{\bar{\alpha}_\ell[n]\}_{n=0}^{N-1}, \nu_\ell, \lambda_\ell \right\}_{\ell=0}^{L_h-1} \tag{8}$$

collects the physical channel parameters.

The sampled received block is therefore

$$\mathbf{y} = \mathbf{H}(\boldsymbol{\epsilon}, \mathbf{h})\mathbf{b} + \mathbf{n}. \tag{9}$$

Conditioned on the physical state and available side information, we assume that $\mathbf{n}$ is zero-mean proper complex noise, is uncorrelated with $\mathbf{b}$ in both the covariance and pseudo-covariance senses, and has covariance $\mathbf{R}_n^{\text{true}} \succ \mathbf{0}$. The numerical experiments use conditionally Gaussian noise, $\mathbf{n} \sim \mathcal{CN}(\mathbf{0}, \mathbf{R}_n^{\text{true}})$, while the linear-MMSE results require only these second-order assumptions. For compactness, define the true physical state as

$$\boldsymbol{\theta} \triangleq \left(\boldsymbol{\epsilon}, \mathbf{h}, \mathbf{R}_n^{\text{true}}\right). \tag{10}$$

C. Imperfect Receiver Information

The equalizer does not know $\boldsymbol{\theta}$. Instead, the preceding synchronization and estimation stages provide

$$\mathsf{S} = \left(\widehat{\boldsymbol{\epsilon}}, \widehat{\mathbf{h}}, \widehat{\mathbf{R}}_n, \boldsymbol{\zeta}\right), \tag{11}$$

where the hatted quantities are synchronization, channel, and noise-covariance estimates. The vector $\boldsymbol{\zeta}$ contains reliability descriptors, such as estimated error variances or pilot-quality indicators. The conditional law $p(\boldsymbol{\theta} \mid \mathsf{S})$ describes the remaining physical-state uncertainty without requiring Gaussian or independent estimation errors.

Physical estimation errors induce the structured channel mismatch

$$\mathbf{E}_H(\boldsymbol{\theta}, \mathsf{S}) = \mathbf{H}(\boldsymbol{\epsilon}, \mathbf{h}) - \mathbf{H}(\widehat{\boldsymbol{\epsilon}}, \widehat{\mathbf{h}}), \tag{12}$$

rather than an arbitrary matrix perturbation. We assume that $\mathbf{b}$ is independent of $(\boldsymbol{\theta}, \mathsf{S})$, so its conditional moments equal the unconditional moments defined above. The side information is obtained from a statistically separate pilot or preamble.

The formulation also covers a selected linear target $\mathbf{t} = \mathbf{A}\mathbf{b}$. The corresponding moments are $\boldsymbol{\mu}_t = \mathbf{A}\boldsymbol{\mu}_b$, $\mathbf{R}_t = \mathbf{A}\mathbf{R}_b\mathbf{A}^H$, and $\mathbf{C}_{y,t}(\boldsymbol{\theta}) = \mathbf{C}(\boldsymbol{\theta})\mathbf{A}^H$, where $\mathbf{C}(\boldsymbol{\theta})$ is defined below. The same substitutions apply to conditional and finite-state moments, and the MSE criterion becomes $\mathbb{E}\|\mathbf{t} - \widehat{\mathbf{t}}\|_2^2$. In the numerical experiments, the target consists of two phase-derotated dominant Laurent coefficients.

D. Augmented Observation Statistics

WL processing augments $\mathbf{y} \in \mathbb{C}^N$ with its conjugate:

$$\underline{\mathbf{y}} = \begin{bmatrix} \mathbf{y} \\ \mathbf{y}^* \end{bmatrix}, \quad \underline{\mathbf{y}} \in \mathbb{C}^{2N}. \tag{13}$$

For a fixed physical state $\boldsymbol{\theta}$, the conditional mean of the augmented observation is

$$\boldsymbol{\mu}_y(\boldsymbol{\theta}) = \mathbb{E}[\underline{\mathbf{y}} \mid \boldsymbol{\theta}] = \begin{bmatrix} \mathbf{H}\boldsymbol{\mu}_b \\ \mathbf{H}^*\boldsymbol{\mu}_b^* \end{bmatrix}, \tag{14}$$

where $\mathbf{H} = \mathbf{H}(\boldsymbol{\epsilon}, \mathbf{h})$.

Define the centered observation–symbol cross-covariance as

$$\mathbf{C}(\boldsymbol{\theta}) = \mathbb{E}\left[(\underline{\mathbf{y}} - \boldsymbol{\mu}_y(\boldsymbol{\theta}))(\mathbf{b} - \boldsymbol{\mu}_b)^H \mid \boldsymbol{\theta}\right] = \begin{bmatrix} \mathbf{H}\mathbf{R}_b \\ \mathbf{H}^*\mathbf{C}_b^* \end{bmatrix}, \tag{15}$$

and the centered augmented observation covariance as

$$\mathbf{R}_y(\boldsymbol{\theta}) = \mathrm{Cov}(\underline{\mathbf{y}} \mid \boldsymbol{\theta}) = \begin{bmatrix} \mathbf{P}(\boldsymbol{\theta}) & \mathbf{Q}(\boldsymbol{\theta}) \\ \mathbf{Q}^*(\boldsymbol{\theta}) & \mathbf{P}^*(\boldsymbol{\theta}) \end{bmatrix}, \tag{16}$$

with

$$\mathbf{P}(\boldsymbol{\theta}) = \mathbf{H}\mathbf{R}_b\mathbf{H}^H + \mathbf{R}_n^{\text{true}}, \qquad \mathbf{Q}(\boldsymbol{\theta}) = \mathbf{H}\mathbf{C}_b\mathbf{H}^T. \tag{17}$$

Given S, the conditional statistics used by the equalizer are

$$\begin{aligned} \boldsymbol{\mu}_\mathsf{S} &= \mathbb{E}[\underline{\mathbf{y}} \mid \mathsf{S}], \quad \mathbf{R}_\mathsf{S} = \mathrm{Cov}(\underline{\mathbf{y}} \mid \mathsf{S}), \\ \mathbf{C}_\mathsf{S} &= \mathbb{E}\left[(\underline{\mathbf{y}} - \boldsymbol{\mu}_\mathsf{S})(\mathbf{b} - \boldsymbol{\mu}_b)^H \mid \mathsf{S}\right]. \end{aligned} \tag{18}$$

Uncertainty in the state-dependent mean also contributes to $\mathbf{R}_\mathsf{S}$. Lemma 1 gives the corresponding decomposition.

E. Receiver Classes

Given S, consider affine-WL receivers of the form

$$\begin{aligned} \widehat{\mathbf{b}} &= \mathbf{a}(\mathsf{S}) + \mathbf{F}(\mathsf{S})^H\mathbf{y} + \mathbf{G}(\mathsf{S})^H\mathbf{y}^* \\ &= \mathbf{a}(\mathsf{S}) + \mathbf{W}(\mathsf{S})^H\underline{\mathbf{y}}, \end{aligned} \tag{19}$$

where

$$\mathbf{W}(\mathsf{S}) = \begin{bmatrix} \mathbf{F}(\mathsf{S}) \\ \mathbf{G}(\mathsf{S}) \end{bmatrix}. \tag{20}$$

Setting $\mathbf{G} = \mathbf{0}$ gives complex-linear processing. The optimal offset vanishes when the conditional target and observation means are both zero. The plug-in (PI) receiver treats the estimated state as exact. It forms $\widehat{\boldsymbol{\theta}} = (\widehat{\boldsymbol{\epsilon}}, \widehat{\mathbf{h}}, \widehat{\mathbf{R}}_n)$ and, assuming $\mathbf{R}_y(\widehat{\boldsymbol{\theta}}) \succ \mathbf{0}$, uses

$$\mathbf{W}_{\text{PI}}(\mathsf{S}) = \mathbf{R}_y(\widehat{\boldsymbol{\theta}})^{-1}\mathbf{C}(\widehat{\boldsymbol{\theta}}), \tag{21}$$

$$\mathbf{a}_{\text{PI}}(\mathsf{S}) = \boldsymbol{\mu}_b - \mathbf{W}_{\text{PI}}(\mathsf{S})^H\boldsymbol{\mu}_y(\widehat{\boldsymbol{\theta}}). \tag{22}$$

This point-estimate design follows the WLTV-MMSE receiver class considered in [1]. To assess the benefit of conjugate processing under synchronization mismatch, we compare it with a complex-linear plug-in LTV-MMSE receiver designed from the same estimated state.

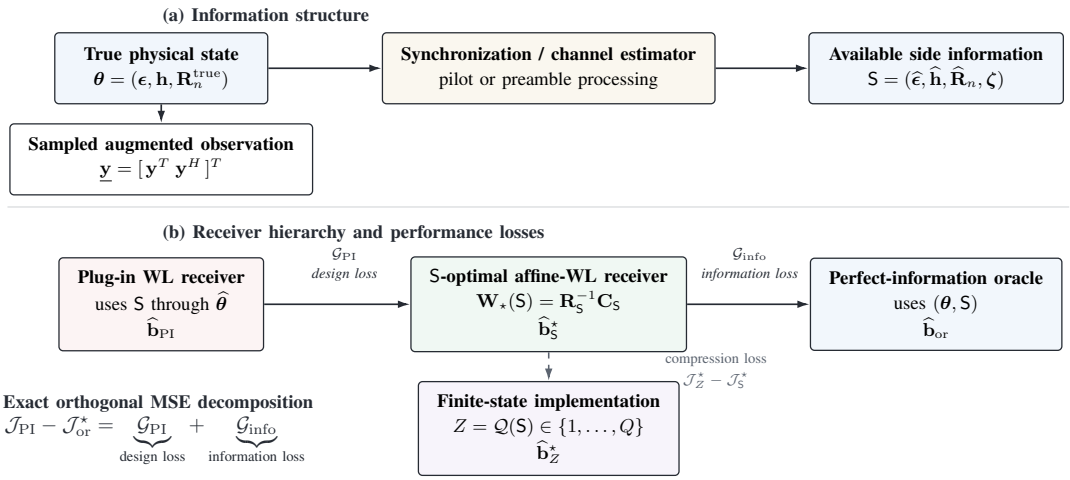


Fig. 1. Information structure and affine-WL receiver hierarchy. The physical state governs the received data and pilot/preamble observations. Conditional adaptation and revelation of the true state remove orthogonal design and information losses, respectively. Compressing side information to Q receiver states trades adaptation accuracy for stored-filter implementation.

Let

$$\widehat{\mathbf{H}} = \mathbf{H}(\widehat{\boldsymbol{\epsilon}}, \widehat{\mathbf{h}}), \qquad \widehat{\mathbf{P}} = \widehat{\mathbf{H}}\mathbf{R}_b\widehat{\mathbf{H}}^H + \widehat{\mathbf{R}}_n, \tag{23}$$

where $\widehat{\mathbf{P}}$ is the plug-in covariance of $\mathbf{y}$.

Assuming $\widehat{\mathbf{P}} \succ \mathbf{0}$, define the complex-linear reference receiver as

$$\widehat{\mathbf{b}}_{\text{r}} = \mathbf{a}_{\text{r}} + \mathbf{F}_{\text{r}}^H\mathbf{y}, \tag{24}$$

where

$$\mathbf{F}_{\text{r}} = \widehat{\mathbf{P}}^{-1}\widehat{\mathbf{H}}\mathbf{R}_b, \qquad \mathbf{a}_{\text{r}} = \boldsymbol{\mu}_b - \mathbf{F}_{\text{r}}^H\widehat{\mathbf{H}}\boldsymbol{\mu}_b. \tag{25}$$

Thus, $\mathbf{G}_{\text{r}} = \mathbf{0}$. In the local viability analysis, both plug-in receivers are frozen at $\mathsf{S} = s$ while the true synchronization state varies.

Let $\mathcal{A}_{\mathsf{S}}$ denote the class of all affine-WL receivers with S-measurable coefficients and estimates with finite second moments. This class allows full use of $\boldsymbol{\zeta}$ without imposing a plug-in structure. The oracle class $\mathcal{A}_{\text{or}}$ allows coefficients measurable with respect to $\mathsf{O} = (\boldsymbol{\theta}, \mathsf{S})$, so $\mathcal{A}_{\mathsf{S}} \subseteq \mathcal{A}_{\text{or}}$. Both classes use the same sampled affine-WL architecture.

F. Problem Formulation

For an affine-WL receiver $\mathcal{R} = (\mathbf{a}, \mathbf{W}) \in \mathcal{A}_{\mathsf{S}}$, define

$$\mathcal{J}(\mathcal{R}) = \mathbb{E}\left[\left\|\mathbf{b} - \mathbf{a}(\mathsf{S}) - \mathbf{W}(\mathsf{S})^H\underline{\mathbf{y}}\right\|_2^2\right]. \tag{26}$$

The side-information and perfect-information affine-WL limits are, respectively,

$$\mathcal{J}_{\mathsf{S}}^\star = \inf_{\mathcal{R}\in\mathcal{A}_{\mathsf{S}}} \mathcal{J}(\mathcal{R}), \tag{27}$$

$$\mathcal{J}_{\text{or}}^\star = \inf_{\mathcal{R}\in\mathcal{A}_{\text{or}}} \mathcal{J}(\mathcal{R}). \tag{28}$$

The information and plug-in design losses are

$$\mathcal{G}_{\text{info}} = \mathcal{J}_{\mathsf{S}}^\star - \mathcal{J}_{\text{or}}^\star, \tag{29}$$

$$\mathcal{G}_{\text{PI}} = \mathcal{J}_{\text{PI}} - \mathcal{J}_{\mathsf{S}}^\star, \tag{30}$$

where $\mathcal{J}_{\text{PI}} = \mathcal{J}(\mathbf{a}_{\text{PI}}, \mathbf{W}_{\text{PI}})$. Consequently,

$$\mathcal{J}_{\text{PI}} - \mathcal{J}_{\text{or}}^\star = \mathcal{G}_{\text{PI}} + \mathcal{G}_{\text{info}}. \tag{31}$$

Section III gives the exact orthogonal MSE interpretation of these losses.

For the synchronization-robustness analysis, we freeze both plug-in receivers at the same estimated state $\widehat{\boldsymbol{\theta}}(s)$. Let $\boldsymbol{\xi} \triangleq (\mathbf{h}, \mathbf{R}_n^{\text{true}})$ collect the physical quantities held fixed while the residual synchronization vector $\boldsymbol{\epsilon}$ varies. For a fixed affine receiver $\mathcal{R}$, define

$$M_{\mathcal{R}}(\boldsymbol{\epsilon}; \boldsymbol{\xi}) = \mathbb{E}\left[\|\mathbf{b} - \widehat{\mathbf{b}}\|_2^2 \mid \boldsymbol{\epsilon}, \boldsymbol{\xi}\right]. \tag{32}$$

The synchronization viability region of the plug-in WLTV receiver is

$$\mathcal{V}_s(\boldsymbol{\xi}) = \{\boldsymbol{\epsilon} : M_{\mathcal{R}_{\text{PI}}}(\boldsymbol{\epsilon}; \boldsymbol{\xi}) < M_{\mathcal{R}_{\text{r}}}(\boldsymbol{\epsilon}; \boldsymbol{\xi})\}, \tag{33}$$

where $\mathcal{R}_{\text{r}}$ is the complex-linear reference receiver. Thus, $\mathcal{V}_s(\boldsymbol{\xi})$ identifies the synchronization states for which the frozen WLTV receiver achieves lower MSE than its complex-linear counterpart. Figure 1 summarizes the information structure and receiver hierarchy.

III. Performance Limits and Receiver Design

We first establish the conditional affine-WL statistics and quantify the local synchronization tolerance of frozen plug-in receivers. We then characterize the side-information and oracle performance limits and use these results to design finite-state receivers. Proofs are provided in the supplementary appendices.

A. Statistical Preliminaries

Using the augmented statistics of Section II-D, we make the following assumptions.

A1) Conditional data statistics: almost surely, $\mathbb{E}[\mathbf{b} \mid \boldsymbol{\theta}, \mathsf{S}] = \boldsymbol{\mu}_b$, with conditional covariance $\mathbf{R}_b$ and pseudo-covariance $\mathbf{C}_b$.

A2) Data-block noise: conditioned on $(\boldsymbol{\theta}, \mathsf{S})$, the noise is zero-mean and proper, has covariance $\mathbf{R}_n^{\mathrm{true}}$, and is uncorrelated with the centered data in both the covariance and pseudo-covariance senses.

A3) Uniform noise floor: there exists $\sigma_0^2 > 0$ such that $\mathbf{R}_n^{\mathrm{true}} \succeq \sigma_0^2 \mathbf{I}$ almost surely.

A4) Finite second moments: $\mathbb{E}\|\mathbf{b}\|_2^2 < \infty$ and $\mathbb{E}\|\underline{\mathbf{y}}\|_2^2 < \infty$.

We impose no Gaussianity or independence assumptions on the timing, frequency, channel, or noise-covariance estimation errors. Their joint uncertainty is described by $p(\boldsymbol{\theta} \mid \mathsf{S})$.

Lemma 1. *Under A1–A4, the observation statistics conditioned on the available side information satisfy* $\boldsymbol{\mu}_{\mathsf{S}} = \mathbb{E}[\boldsymbol{\mu}_y(\boldsymbol{\theta}) \mid \mathsf{S}]$ *and* $\mathbf{C}_{\mathsf{S}} = \mathbb{E}[\mathbf{C}(\boldsymbol{\theta}) \mid \mathsf{S}]$. *The observation covariance decomposes as*

$$\mathbf{R}_{\mathsf{S}} = \mathbb{E}[\mathbf{R}_y(\boldsymbol{\theta}) \mid \mathsf{S}] + \mathrm{Cov}\left(\boldsymbol{\mu}_y(\boldsymbol{\theta}) \mid \mathsf{S}\right), \tag{34}$$

and $\mathbf{R}_{\mathsf{S}} \succeq \sigma_0^2 \mathbf{I}_{2N}$ *almost surely.*

Proof: See Appendix B.

Thus, the conditional covariance accounts for both the average physical-state covariance and variation in the state-dependent mean. Evaluating the statistics at a single state estimate generally does not capture these effects.

B. Conditional Affine-WL Estimation

Let U denote side information satisfying $\mathbb{E}[\mathbf{b} \mid U] = \boldsymbol{\mu}_b$ and $\mathrm{Cov}(\mathbf{b} \mid U) = \mathbf{R}_b$ almost surely, and consider $\widehat{\mathbf{b}} = \mathbf{a}(U) + \mathbf{W}(U)^H \underline{\mathbf{y}}$. Define $\boldsymbol{\mu}_U = \mathbb{E}[\underline{\mathbf{y}} \mid U]$, $\mathbf{R}_U = \mathrm{Cov}(\underline{\mathbf{y}} \mid U)$, and $\mathbf{C}_U = \mathbb{E}[(\underline{\mathbf{y}} - \boldsymbol{\mu}_U)(\mathbf{b} - \boldsymbol{\mu}_b)^H \mid U]$. The following identity applies to the available information $U = \mathsf{S}$, its finite-state representation $U = Z = \mathcal{Q}(\mathsf{S})$, and the oracle information $U = \mathsf{O} = (\boldsymbol{\theta}, \mathsf{S})$.

Lemma 2 (Conditional affine-WL MSE)**.** *For any admissible offset* $\mathbf{a}(U)$ *and filter* $\mathbf{W}(U)$,

$$\begin{aligned} \mathcal{J}(\mathbf{a}, \mathbf{W} \mid U) &\triangleq \mathbb{E}\big[\|\mathbf{b} - \mathbf{a} - \mathbf{W}^H \underline{\mathbf{y}}\|_2^2 \mid U\big] \\ &= \mathrm{tr}(\mathbf{R}_b) + \|\boldsymbol{\mu}_b - \mathbf{a} - \mathbf{W}^H \boldsymbol{\mu}_U\|_2^2 \\ &\quad - 2\Re\big\{\mathrm{tr}(\mathbf{W}^H \mathbf{C}_U)\big\} + \mathrm{tr}(\mathbf{W}^H \mathbf{R}_U \mathbf{W}) \end{aligned} \tag{35}$$

almost surely. For a fixed $\mathbf{W}(U)$*, the MSE-minimizing offset is*

$$\mathbf{a}(U) = \boldsymbol{\mu}_b - \mathbf{W}(U)^H \boldsymbol{\mu}_U.$$

Proof: See Appendix C.

C. Local Timing–Frequency Viability of the Plug-In Receiver

We first quantify the synchronization mismatch over which a frozen plug-in WLTV receiver retains its MSE advantage over the complex-linear reference. Fix $\mathsf{S} = s$, the receivers $\mathcal{R}_{\mathrm{PI}}$ and $\mathcal{R}_{\mathrm{r}}$, the design point $\boldsymbol{\epsilon}_0 = \widehat{\boldsymbol{\epsilon}}(s)$, and the physical quantities $\boldsymbol{\xi} = (\mathbf{h}, \mathbf{R}_n^{\mathrm{true}})$. Only $\boldsymbol{\epsilon} = (\epsilon_\tau, \epsilon_\nu)^T$ varies.

Write $\widehat{\boldsymbol{\theta}} = (\widehat{\boldsymbol{\epsilon}}, \widehat{\mathbf{h}}, \widehat{\mathbf{R}}_n)$ for the estimated state, and let $\widehat{\boldsymbol{\mu}}_y = \boldsymbol{\mu}_y(\widehat{\boldsymbol{\theta}})$, $\widehat{\mathbf{R}}_y = \mathbf{R}_y(\widehat{\boldsymbol{\theta}})$, and $\widehat{\mathbf{C}} = \mathbf{C}(\widehat{\boldsymbol{\theta}})$ denote the corresponding statistics. Provided $\widehat{\mathbf{R}}_y \succ \mathbf{0}$, the plug-in WLTV receiver uses

$$\mathbf{W}_{\mathrm{PI}} = \widehat{\mathbf{R}}_y^{-1} \widehat{\mathbf{C}}, \qquad \mathbf{a}_{\mathrm{PI}} = \boldsymbol{\mu}_b - \mathbf{W}_{\mathrm{PI}}^H \widehat{\boldsymbol{\mu}}_y. \tag{36}$$

The complex-linear reference $\mathcal{R}_{\mathrm{r}}$ in (24)–(25) is designed from the same $\widehat{\boldsymbol{\theta}}$ and held fixed in the same way. The comparison therefore isolates the benefit of WL processing under a common synchronization mismatch.

The channel depends on $\boldsymbol{\epsilon}$ through the pulse shift and common residual-frequency phase in (7). For differentiable effective pulses, define $\eta = T_s/T$ and $\mathbf{D} = \mathrm{diag}(t_0/T_s, t_0/T_s + 1, \ldots, t_0/T_s + N - 1)$. Using subscripts τ and ν for derivatives with respect to ϵ_τ and ϵ_ν, respectively, the first channel derivatives are

$$\begin{aligned} [\mathbf{H}_\tau]_{n,k} &= -T \sum_{\ell=0}^{L_h - 1} \bar{\alpha}_\ell[n]\, e^{j2\pi(t_0 + nT_s)(\nu_\ell + \epsilon_\nu/T)} \\ &\quad \times \phi_k'(nT_s - \lambda_\ell - T\epsilon_\tau), \\ \mathbf{H}_\nu &= j2\pi\eta \mathbf{D}\mathbf{H}. \end{aligned} \tag{37}$$

The corresponding derivatives of $\boldsymbol{\mu}_y$, $\mathbf{C}$, and $\mathbf{R}_y$, together with the first- and second-order MSE derivatives used below, are given in Appendix A.

For a fixed affine receiver $\mathcal{R} = (\mathbf{a}, \mathbf{W})$, define $\mathbf{m}_{\mathcal{R}} = \boldsymbol{\mu}_b - \mathbf{a} - \mathbf{W}^H \boldsymbol{\mu}_y$. Its pointwise MSE is

$$\begin{aligned} M_{\mathcal{R}}(\boldsymbol{\epsilon}; \boldsymbol{\xi}) &= \mathrm{tr}(\mathbf{R}_b) + \|\mathbf{m}_{\mathcal{R}}\|_2^2 - 2\Re\{\mathrm{tr}(\mathbf{W}^H \mathbf{C})\} \\ &\quad + \mathrm{tr}(\mathbf{W}^H \mathbf{R}_y \mathbf{W}). \end{aligned} \tag{38}$$

Because the receiver coefficients are fixed, the gradient and Hessian with respect to $\boldsymbol{\epsilon}$ depend only on derivatives of the state-dependent statistics.

Define the relative MSE as

$$D_s(\boldsymbol{\epsilon}; \boldsymbol{\xi}) = M_{\mathcal{R}_{\mathrm{PI}}}(\boldsymbol{\epsilon}; \boldsymbol{\xi}) - M_{\mathcal{R}_{\mathrm{r}}}(\boldsymbol{\epsilon}; \boldsymbol{\xi}).$$

The exact viability region is $\mathcal{V}_s(\boldsymbol{\xi}) = \{\boldsymbol{\epsilon} : D_s(\boldsymbol{\epsilon}; \boldsymbol{\xi}) < 0\}$. At $\boldsymbol{\epsilon}_0$, define the nominal margin $\Gamma_s = -D_s(\boldsymbol{\epsilon}_0; \boldsymbol{\xi})$, sensitivity $\mathbf{g}_s = \nabla_{\boldsymbol{\epsilon}} D_s(\boldsymbol{\epsilon}_0; \boldsymbol{\xi})$, and curvature $\mathbf{B}_s = \nabla_{\boldsymbol{\epsilon}}^2 D_s(\boldsymbol{\epsilon}_0; \boldsymbol{\xi})$. These derivatives follow from (70)–(71) by subtracting the reference-receiver derivatives from those of the plug-in WLTV receiver.

Theorem 1 (Local relative-MSE viability)**.** *Fix* $\mathsf{S} = s$ *and* $\boldsymbol{\xi}$*. Suppose* $D_s(\boldsymbol{\epsilon}; \boldsymbol{\xi})$ *is three times continuously*

differentiable in a neighborhood of $\boldsymbol{\epsilon}_0$, and $\Gamma_s > 0$. For $\boldsymbol{\delta} = \boldsymbol{\epsilon} - \boldsymbol{\epsilon}_0$, define

$$q_s(\boldsymbol{\delta}) \triangleq -\Gamma_s + \mathbf{g}_s^T\boldsymbol{\delta} + \frac{1}{2}\boldsymbol{\delta}^T\mathbf{B}_s\boldsymbol{\delta}.$$

For sufficiently small $\boldsymbol{\delta}$,

$$D_s(\boldsymbol{\epsilon}_0 + \boldsymbol{\delta}; \boldsymbol{\xi}) = q_s(\boldsymbol{\delta}) + R_3(\boldsymbol{\delta}), \tag{39}$$

where R_3 is the third-order remainder and $D_s(\boldsymbol{\epsilon}_0; \boldsymbol{\xi}) = -\Gamma_s < 0$.

Let $\mathcal{B}_r = \{\boldsymbol{\delta} : \|\boldsymbol{\delta}\|_2 \le r\}$ for $r > 0$ such that $\boldsymbol{\epsilon}_0 + \mathcal{B}_r$ lies within this neighborhood. Define

$$L_3(r) \triangleq \sup_{\boldsymbol{\delta}\in\mathcal{B}_r} \left\|\nabla^3_{\boldsymbol{\epsilon}} D_s(\boldsymbol{\epsilon}_0 + \boldsymbol{\delta}; \boldsymbol{\xi})\right\|_{\mathrm{op}},$$

where

$$\|\nabla^3_{\boldsymbol{\epsilon}} D_s(\mathbf{x}; \boldsymbol{\xi})\|_{\mathrm{op}} \triangleq \sup_{\substack{\|\mathbf{u}\|_2=\|\mathbf{v}\|_2=1\\ \|\mathbf{w}\|_2=1}} \left|\nabla^3_{\boldsymbol{\epsilon}} D_s(\mathbf{x}; \boldsymbol{\xi})[\mathbf{u}, \mathbf{v}, \mathbf{w}]\right|.$$

For finite $L_3(r)$, Taylor's theorem gives $|R_3(\boldsymbol{\delta})| \le L_3(r)\|\boldsymbol{\delta}\|_2^3/6$ on $\mathcal{B}_r$.

Define the inner and outer regions

$$\mathcal{V}_{\mathrm{in}}(r) = \{\boldsymbol{\epsilon}_0 + \boldsymbol{\delta} : \|\boldsymbol{\delta}\|_2 \le r, \; q_s(\boldsymbol{\delta}) + \frac{L_3(r)}{6}\|\boldsymbol{\delta}\|_2^3 < 0\}, \tag{40}$$

$$\mathcal{V}_{\mathrm{out}}(r) = \{\boldsymbol{\epsilon}_0 + \boldsymbol{\delta} : \|\boldsymbol{\delta}\|_2 \le r, \; q_s(\boldsymbol{\delta}) - \frac{L_3(r)}{6}\|\boldsymbol{\delta}\|_2^3 < 0\}. \tag{41}$$

Then

$$\mathcal{V}_{\mathrm{in}}(r) \subseteq \mathcal{V}_s(\boldsymbol{\xi}) \cap (\boldsymbol{\epsilon}_0 + \mathcal{B}_r) \subseteq \mathcal{V}_{\mathrm{out}}(r). \tag{42}$$

The inner region certifies retained WL advantage, while the outer region contains every viable point within radius r.

Proof: See Appendix D.

Neglecting the remainder gives the approximate local boundary

$$\mathbf{g}_s^T\boldsymbol{\delta} + \frac{1}{2}\boldsymbol{\delta}^T\mathbf{B}_s\boldsymbol{\delta} = \Gamma_s, \tag{43}$$

where Γ_s, $\mathbf{g}_s$, and $\mathbf{B}_s$ describe the nominal WL advantage, sensitivity, and curvature, respectively. If $\mathbf{B}_s \succ \mathbf{0}$, this boundary is an ellipse centered at $-\mathbf{B}_s^{-1}\mathbf{g}_s$ in $\boldsymbol{\delta}$-coordinates. The certified regions additionally account for the remainder.

A sufficient condition for every point in $\boldsymbol{\epsilon}_0 + \mathcal{B}_r$ to remain viable is

$$-\Gamma_s + \|\mathbf{g}_s\|_2 r + \frac{1}{2}\max\{\lambda_{\max}(\mathbf{B}_s), 0\}r^2 + \frac{L_3(r)}{6}r^3 < 0. \tag{44}$$

This condition follows by uniformly bounding the linear and quadratic terms on $\mathcal{B}_r$. It provides an analysis certificate for fixed $\boldsymbol{\xi}$ and a valid upper bound on $L_3(r)$; using it as an online test would require information beyond S.

D. Best Receiver Using the Available Side Information

We next characterize the best affine-WL receiver using S without imposing a plug-in structure. This benchmark identifies the loss that receiver redesign can remove without improving the front-end information. By Lemma 1, $\mathbf{R}_{\mathsf{S}} \succeq \sigma_0^2\mathbf{I}_{2N}$ almost surely.

Theorem 2 (Side-information-optimal affine-WL receiver)**.** *Under A1–A4, the minimum-MSE affine-WL receiver based on S is unique up to almost-sure equality and is given by*

$$\begin{aligned}\widehat{\mathbf{b}}^{\star}_{\mathsf{S}} &= \mathbf{a}_{\star}(\mathsf{S}) + \mathbf{W}_{\star}(\mathsf{S})^H\underline{\mathbf{y}},\\ \mathbf{W}_{\star}(\mathsf{S}) &= \mathbf{R}_{\mathsf{S}}^{-1}\mathbf{C}_{\mathsf{S}},\end{aligned} \tag{45}$$

with $\mathbf{a}_{\star}(\mathsf{S}) = \boldsymbol{\mu}_b - \mathbf{W}_{\star}(\mathsf{S})^H\boldsymbol{\mu}_{\mathsf{S}}$. Its minimum unconditional MSE is

$$\mathcal{J}^{\star}_{\mathsf{S}} = \mathrm{tr}(\mathbf{R}_b) - \mathbb{E}\big[\mathrm{tr}\big(\mathbf{C}_{\mathsf{S}}^H\mathbf{R}_{\mathsf{S}}^{-1}\mathbf{C}_{\mathsf{S}}\big)\big]. \tag{46}$$

For any other admissible affine-WL receiver $(\mathbf{a}(\mathsf{S}), \mathbf{W}(\mathsf{S}))$ using the same side information, the excess MSE is

$$\begin{aligned}\mathcal{J}(\mathbf{a}, \mathbf{W}) - \mathcal{J}^{\star}_{\mathsf{S}} = \mathbb{E}\Big[&\|\boldsymbol{\mu}_b - \mathbf{a} - \mathbf{W}^H\boldsymbol{\mu}_{\mathsf{S}}\|_2^2\\ &+ \mathrm{tr}\big((\mathbf{W} - \mathbf{W}_{\star})^H\mathbf{R}_{\mathsf{S}}(\mathbf{W} - \mathbf{W}_{\star})\big)\Big].\end{aligned} \tag{47}$$

Both terms are nonnegative and quantify the penalties due to mean mismatch and filter mismatch, respectively.

Proof: See Appendix E.

The classical affine/WL-MMSE projection [4], [17], [18] therefore gives an architecture-specific performance limit using conditional moments over the physical states compatible with S.

The distinction from posterior-mean parameter substitution is already visible when $\boldsymbol{\mu}_b = \mathbf{0}$. Define $\overline{\mathbf{H}}_{\mathsf{S}} = \mathbb{E}[\mathbf{H} \mid \mathsf{S}]$ and $\Delta\mathbf{H} = \mathbf{H} - \overline{\mathbf{H}}_{\mathsf{S}}$. The ordinary covariance block satisfies

$$\begin{aligned}\mathbb{E}[\mathbf{P}(\boldsymbol{\theta}) \mid \mathsf{S}] = \overline{\mathbf{H}}_{\mathsf{S}}\mathbf{R}_b\overline{\mathbf{H}}_{\mathsf{S}}^H &+ \mathbb{E}[\Delta\mathbf{H}\mathbf{R}_b\Delta\mathbf{H}^H \mid \mathsf{S}]\\ &+ \mathbb{E}[\mathbf{R}_n^{\mathrm{true}} \mid \mathsf{S}],\end{aligned} \tag{48}$$

while the complementary covariance block is

$$\begin{aligned}\mathbb{E}[\mathbf{Q}(\boldsymbol{\theta}) \mid \mathsf{S}] = \overline{\mathbf{H}}_{\mathsf{S}}\mathbf{C}_b\overline{\mathbf{H}}_{\mathsf{S}}^T&\\ + \mathbb{E}[\Delta\mathbf{H}\mathbf{C}_b\Delta\mathbf{H}^T \mid \mathsf{S}].&\end{aligned} \tag{49}$$

Thus, even substituting the conditional mean channel omits uncertainty-dependent covariance terms. Moreover, because $\mathbf{H}(\boldsymbol{\epsilon}, \mathbf{h})$ is nonlinear in the physical parameters,

$$\mathbf{H}(\mathbb{E}[\boldsymbol{\epsilon} \mid \mathsf{S}], \mathbb{E}[\mathbf{h} \mid \mathsf{S}]) \neq \mathbb{E}[\mathbf{H}(\boldsymbol{\epsilon}, \mathbf{h}) \mid \mathsf{S}]$$

in general.

For the plug-in receiver, (47) gives

$$\mathcal{G}_{\mathrm{PI}} = \mathbb{E}\Big[\|\mathbf{W}_{\mathrm{PI}}^H(\widehat{\boldsymbol{\mu}}_y - \boldsymbol{\mu}_{\mathsf{S}})\|_2^2 + \mathrm{tr}\big((\mathbf{W}_{\mathrm{PI}} - \mathbf{W}_\star)^H \mathbf{R}_{\mathsf{S}}(\mathbf{W}_{\mathrm{PI}} - \mathbf{W}_\star)\big)\Big] \geq 0. \tag{50}$$

The first term penalizes the use of the point-estimate mean in place of the conditional mean; the second penalizes filter mismatch. Hence, $\mathcal{G}_{\mathrm{PI}}$ is a pure *design loss*: it can be reduced while retaining the same front-end information.

E. Oracle Performance and Design–Information Decomposition

Let $\mathsf{O} = (\boldsymbol{\theta}, \mathsf{S})$ additionally reveal the physical state. Because O includes S, every S-based receiver is oracle-admissible. Under A1–A2, the observation statistics conditioned on O are $\boldsymbol{\mu}_y(\boldsymbol{\theta})$, $\mathbf{R}_y(\boldsymbol{\theta})$, and $\mathbf{C}(\boldsymbol{\theta})$. The oracle provides a perfect-information benchmark within the same sampled affine-WL architecture.

Theorem 3 (Oracle receiver and orthogonal loss decomposition)**.** *Under A1–A4, the minimum-MSE affine-WL receiver based on $\mathsf{O} = (\boldsymbol{\theta}, \mathsf{S})$ is*

$$\begin{aligned} \widehat{\mathbf{b}}_{\mathrm{or}} &= \mathbf{a}_{\mathrm{or}}(\boldsymbol{\theta}) + \mathbf{W}_{\mathrm{or}}(\boldsymbol{\theta})^H \underline{\mathbf{y}}, \\ \mathbf{W}_{\mathrm{or}}(\boldsymbol{\theta}) &= \mathbf{R}_y(\boldsymbol{\theta})^{-1}\mathbf{C}(\boldsymbol{\theta}), \end{aligned} \tag{51}$$

where $\mathbf{a}_{\mathrm{or}}(\boldsymbol{\theta}) = \boldsymbol{\mu}_b - \mathbf{W}_{\mathrm{or}}(\boldsymbol{\theta})^H \boldsymbol{\mu}_y(\boldsymbol{\theta})$. Its average MSE is

$$\mathcal{J}_{\mathrm{or}}^\star = \mathrm{tr}(\mathbf{R}_b) - \mathbb{E}\big[\mathrm{tr}\big(\mathbf{C}(\boldsymbol{\theta})^H \mathbf{R}_y(\boldsymbol{\theta})^{-1}\mathbf{C}(\boldsymbol{\theta})\big)\big]. \tag{52}$$

The information gap $\mathcal{G}_{\mathrm{info}} = \mathcal{J}_{\mathsf{S}}^\star - \mathcal{J}_{\mathrm{or}}^\star$ satisfies

$$\mathcal{G}_{\mathrm{info}} = \mathbb{E}\Big[\|\widehat{\mathbf{b}}_{\mathsf{S}}^\star - \widehat{\mathbf{b}}_{\mathrm{or}}\|_2^2\Big] \geq 0. \tag{53}$$

Thus, the loss due to incomplete physical-state information equals the mean-square distance between the side-information-optimal and oracle affine-WL estimates.

The total degradation of the plug-in receiver relative to the oracle satisfies

$$\mathcal{J}_{\mathrm{PI}} - \mathcal{J}_{\mathrm{or}}^\star = \mathcal{G}_{\mathrm{PI}} + \mathcal{G}_{\mathrm{info}}, \tag{54}$$

and the corresponding estimator corrections are orthogonal in the unconditional mean-square sense:

$$\mathbb{E}\Big[(\widehat{\mathbf{b}}_{\mathrm{PI}} - \widehat{\mathbf{b}}_{\mathsf{S}}^\star)^H(\widehat{\mathbf{b}}_{\mathsf{S}}^\star - \widehat{\mathbf{b}}_{\mathrm{or}})\Big] = 0. \tag{55}$$

Proof: See Appendix F.

Equation (55) separates the benefit of receiver redesign using unchanged side information from the benefit of revealing the physical state.

Equivalently,

$$\mathcal{G}_{\mathrm{info}} = \mathbb{E}\Big[\|\mathbf{W}_\star^H(\boldsymbol{\mu}_y(\boldsymbol{\theta}) - \boldsymbol{\mu}_{\mathsf{S}})\|_2^2 + \mathrm{tr}\big((\mathbf{W}_\star - \mathbf{W}_{\mathrm{or}})^H \mathbf{R}_y(\boldsymbol{\theta})(\mathbf{W}_\star - \mathbf{W}_{\mathrm{or}})\big)\Big]. \tag{56}$$

Information loss therefore arises from uncertainty in the state-dependent observation mean, the optimal WL coefficient matrix, or both. A dominant $\mathcal{G}_{\mathrm{PI}}$ indicates greater potential benefit from equalizer redesign, whereas a dominant $\mathcal{G}_{\mathrm{info}}$ indicates greater potential benefit from more informative front-end estimation.

Corollary 1 (Zero information loss)**.** *The information gap vanishes if and only if $\widehat{\mathbf{b}}_{\mathsf{S}}^\star = \widehat{\mathbf{b}}_{\mathrm{or}}$ almost surely.*

Proof: See Appendix G.

Zero information loss therefore does not require exact recovery of every physical parameter. It requires only that the remaining state ambiguity leave the optimal affine-WL estimate unchanged, providing a receiver-oriented notion of sufficient front-end information.

F. Finite-State Approximation

Continuous adaptation of $(\mathbf{a}_\star(\mathsf{S}), \mathbf{W}_\star(\mathsf{S}))$ may require repeated evaluation of conditional statistics and synthesis of filter coefficients. A finite-state implementation replaces these online operations with selection from a stored filter bank. Context-tree and clustering turbo equalizers compress decoder side information [11], [12]. Here, $Z = \mathcal{Q}(\mathsf{S}) \in \{1, \ldots, Q\}$ compresses uncertain physical-state information and selects one stored receiver from $\{(\mathbf{a}_j, \mathbf{W}_j)\}_{j=1}^Q$.

For implementation, the state decision can use a lower-dimensional routing feature $\boldsymbol{\psi}(\mathsf{S})$:

$$Z = \widetilde{\mathcal{Q}}(\boldsymbol{\psi}(\mathsf{S})), \qquad Z \in \{1, \ldots, Q\}. \tag{57}$$

Choosing $\boldsymbol{\psi}(\mathsf{S}) = \mathsf{S}$ recovers the unrestricted formulation. Practical features may include synchronization estimates, channel and noise quality indicators, and reliability descriptors in $\boldsymbol{\zeta}$.

For every state j with $\Pr(Z = j) > 0$, define $\boldsymbol{\mu}_j = \mathbb{E}[\underline{\mathbf{y}} \mid Z = j]$, $\mathbf{R}_j = \mathrm{Cov}(\underline{\mathbf{y}} \mid Z = j)$, and

$$\mathbf{C}_j = \mathbb{E}[(\underline{\mathbf{y}} - \boldsymbol{\mu}_j)(\mathbf{b} - \boldsymbol{\mu}_b)^H \mid Z = j].$$

Because Z is a deterministic function of S, A1 and the tower property preserve the target moments when conditioning on Z. Under A1–A4, the conditional covariance decomposition also gives $\mathbf{R}_j \succeq \sigma_0^2 \mathbf{I}_{2N}$. Thus, every state of positive probability admits a unique affine-WL MMSE solution.

Theorem 4 (Optimal finite-state affine-WL receiver and routing-information monotonicity)**.** *For a fixed quantizer $\mathcal{Q}$, the unique minimum-MSE affine-WL receiver for each state j with $\Pr(Z = j) > 0$ is*

$$\mathbf{W}_j^\star = \mathbf{R}_j^{-1}\mathbf{C}_j, \qquad \mathbf{a}_j^\star = \boldsymbol{\mu}_b - (\mathbf{W}_j^\star)^H \boldsymbol{\mu}_j. \tag{58}$$

Let $\widehat{\mathbf{b}}_Z^\star$ denote the estimate obtained by selecting these coefficients according to $Z = \mathcal{Q}(\mathsf{S})$. Then

$$\mathcal{J}_Z^\star - \mathcal{J}_{\mathsf{S}}^\star = \mathbb{E}\left[\left\|\widehat{\mathbf{b}}_Z^\star - \widehat{\mathbf{b}}_{\mathsf{S}}^\star\right\|_2^2\right] \geq 0. \tag{59}$$

Thus, the exact MSE cost of finite-state adaptation equals the mean-square distance between the optimal finite-state and continuously adapted estimates.

More generally, let $\mathfrak{Q}_Q(\psi)$ denote the class of deterministic Q-state quantizers that depend on S only through $\psi(\mathsf{S})$, and define

$$\mathcal{J}^\star_{Q,\psi} \triangleq \inf_{\mathcal{Q}\in\mathfrak{Q}_Q(\psi)} \mathcal{J}^\star_{\mathcal{Q}}, \tag{60}$$

where $\mathcal{J}^\star_{\mathcal{Q}}$ is the MSE obtained using the optimal coefficients in (58) *for the partition induced by $\mathcal{Q}$. Then*

$$\mathcal{J}^\star_{\mathsf{S}} \le \mathcal{J}^\star_{Q,\psi}. \tag{61}$$

If $\psi_1(\mathsf{S}) = g(\psi_2(\mathsf{S}))$ almost surely for some measurable g, then

$$\mathcal{J}^\star_{Q,\psi_2} \le \mathcal{J}^\star_{Q,\psi_1}. \tag{62}$$

Hence, at a fixed state budget Q, adding available reliability information to the routing feature cannot increase the best achievable population MSE.

Proof: See Appendix H.

Nearby parameter values need not yield similar equalizers. We therefore measure the cost of sharing a filter directly through excess MSE. For $\mathsf{S} = s$ and a candidate stored receiver $(\mathbf{a}, \mathbf{W})$, define

$$\begin{aligned} d(s;\mathbf{a},\mathbf{W}) = {} & \left\|\boldsymbol{\mu}_b - \mathbf{a} - \mathbf{W}^H\boldsymbol{\mu}_{\mathsf{S}}(s)\right\|_2^2 \\ & + \mathrm{tr}\Big((\mathbf{W}-\mathbf{W}_\star(s))^H\mathbf{R}_{\mathsf{S}}(s) \\ & \qquad \times (\mathbf{W}-\mathbf{W}_\star(s))\Big). \end{aligned} \tag{63}$$

By Theorem 2, this distortion is the conditional excess MSE relative to continuous adaptation.

Proposition 1 (Generalized Lloyd conditions)**.** *For a fixed codebook $\{(\mathbf{a}_j,\mathbf{W}_j)\}_{j=1}^Q$, an unrestricted MSE-minimizing assignment satisfies*

$$\mathcal{Q}^\star(s) \in \arg\min_{1\le j\le Q} d(s;\mathbf{a}_j,\mathbf{W}_j) \tag{64}$$

for almost every s under the distribution of S.

For a fixed partition of the side-information space, the MSE-minimizing codeword for each state of positive probability is the conditional affine-WL MMSE receiver in (58)*.*

Proof: See Appendix I.

This proposition specializes the classical Lloyd/LBG alternating-minimization principle [19], [20] to the equalization distortion in (63). Alternating minimum-distortion assignments and conditional-MMSE codeword updates produces nonincreasing population MSE values. These values therefore converge, although global optimality is not guaranteed. Finite-sample designs require validation.

The bank is designed offline using a model or training ensemble. To avoid the online conditional-statistic evaluations that exact distortion routing may require, our numerical implementation uses threshold routing with $\psi(\mathsf{S}) = [\widehat{\epsilon}_\tau, \widehat{\epsilon}_\nu, \boldsymbol{\zeta}_{\mathrm{sync}}^T]^T$. Nonuniform thresholds may also initialize Lloyd refinement without changing the observation architecture.

IV. Numerical Evaluation

We evaluate finite-state adaptation against the point-estimate (PI) and posterior-mean (PM) substitution receivers, a matched-budget representative-state bank, a numerical continuous-adaptation reference, and a matched-state/oracle reference. These comparisons quantify the gains from uncertainty-aware coefficient design and the cost of finite-state implementation. Theorem 1 provides the analytical robustness certificate.

A. Simulation Setup

The binary GMSK link operates at 200 kbit/s with symbol duration $T = 5$ μs, carrier frequency 5.06 GHz, modulation index $1/2$, Gaussian-filter bandwidth–time product $BT = 0.30$, memory $L = 3$, and eight samples per symbol. A four-symbol observation window contains 32 complex samples. The known reference channel has delays $(0, 3.5, 7)$ μs, Doppler shifts $(1520, -700, 250)$ Hz, phases $(0, 0.8, -1.1)$, and powers $(\kappa, 0.75, 0.25)/(\kappa+1)$, where $\kappa = 10^{2.9}$. Unless otherwise stated, $t_0 = 60T = 300$ μs; phase rotations use $t_0 + nT_s$, while pulse arguments use nT_s.

The dominant-component implementation retains 18 Laurent coefficients, indexed by $m = -9, \ldots, 8$. Writing $b_m = j^{m+1}u_m$, with equiprobable $u_m \in \{-1, +1\}$, allows the phase rotations to be absorbed into the equivalent real channel matrix $\mathbf{B} \in \mathbb{R}^{64\times 18}$. We estimate $\mathbf{t} = [u_0, u_{-1}]^T$ from $\mathbf{y}_{\mathrm{R}} = [\Re\{\mathbf{y}\}^T \ \Im\{\mathbf{y}\}^T]^T$, an equivalent real representation of augmented WL processing. Each filter has 64×2 real coefficients, and bit decisions use $\mathrm{sign}(\widehat{u}_0\widehat{u}_{-1})$. MSE is averaged over the two target coordinates. Filter design and analytical MSE calculations use the dominant component; empirical full-CPM MSE and ABER use the full waveform. With $\gamma = 10^{(E_b/N_0)_{\mathrm{dB}}/10}$, the complex white-noise variance is $8/\gamma$, and the variance per real coordinate is $n_r = 8/(2\gamma)$.

The true residual timing and common-frequency states, denoted here by τ and f, are independent zero-mean Gaussians with

$$\mathrm{std}(\tau/T) = 0.20, \qquad \mathrm{std}(f) = 400 \text{ Hz}. \tag{65}$$

Independently of these states and the transmitted data, synchronization-estimation errors are zero-mean Gaussian with standard deviations (σ_τ, σ_f). The reported standard deviations equal the actual values except in the miscalibration experiment. The high-uncertainty setting is

$$\sigma_\tau/T = 0.25, \qquad \sigma_f = 500 \text{ Hz}. \tag{66}$$

PI synthesizes its filter at $(\widehat{\tau}, \widehat{f})$. PM first computes the Gaussian posterior-mean state using the same reported uncertainty available to the bank, then substitutes this state into the filter design. The bank routes using features derived from

$$\boldsymbol{\psi}_2 = (\widehat{\tau}, \widehat{f}, \sigma_\tau, \sigma_f). \tag{67}$$

Offline development uses 4500 training states and 1500 independent validation states. Their error standard deviations are drawn independently from log-uniform distributions on $[0.02, 0.35]T$ and $[25, 600]$ Hz. For each Q, candidate empirical-quantile partitions use timing and frequency bin counts whose product is Q, in either raw-estimate or posterior-mean coordinates. Conditional moments are obtained by averaging model moments over training states, with pseudo-symbols averaged analytically. At $E_b/N_0 = 8$ dB, validation MSE selects the conditional-bank partition, after which the bank is refitted using all 6000 development states. At each E_b/N_0, the corresponding noise variance is inserted into the same conditional moments. The evaluated design uses this restricted threshold search; generalized Lloyd refinement and unrestricted population optimization are not performed.

The SNR and state-budget tests use 100 synchronization-state clusters, 800 symbol contexts per cluster, and 800 paired cluster-bootstrap resamples. The channel, age, calibration, and continuous-reference tests use independent seeds, 256 clusters, 400 contexts per cluster at $E_b/N_0 = 8$ dB, and 2000 bootstrap resamples. Receivers share waveform and noise realizations, and test labels are never used to select partitions. Intervals are pointwise, except for the channel-ensemble aggregate, which resamples channels within each power-ratio stratum. The supplied code, seeds, channel parameters, and cluster outputs support reproduction of these tests.

B. Reference-Channel Performance and State Budget

Figure 2 shows reference-channel performance versus E_b/N_0. At $E_b/N_0 = 8$ dB, the bank reduces pseudo-symbol MSE by 51.9% relative to PI, empirical full-CPM MSE from 0.60402 to 0.29175, and ABER from 0.22493 to 0.13404. PM attains 0.31053, 0.31149, and 0.15246 in these three metrics, respectively. The bank therefore provides additional reductions of 6.6%, 6.3%, and 12.1%. Paired 95% intervals for the absolute PM-minus-bank reductions are $[0.01009, 0.03114]$, $[0.00913, 0.03005]$, and $[0.01130, 0.02653]$, respectively. At $E_b/N_0 = 12$ dB, the corresponding relative reductions reach 16.9%, 16.5%, and 26.6%. These results refer to the SNR-test ensemble; the robustness and continuous-reference tests below use independent ensembles.

The PI baseline implements conventional WLTV-MMSE state substitution within the common sampled GMSK model by treating the estimated physical state as exact. The aeronautical CPM/WLTV framework in [1] provides the closest application-specific precedent. The reported gains quantify uncertainty-aware adaptation relative to this controlled PI implementation.

Figure 3 evaluates $Q \in \{1, 2, 4, 8, 16, 32, 64\}$ at $E_b/N_0 = 8$ dB under (66). PI and PM attain pseudo-symbol MSEs of 0.60303 and 0.31053, while the $Q = 16$ and $Q = 64$ banks attain 0.29013 and 0.27939. Thus, $Q = 16$ retains 96.7% of the improvement achieved by $Q = 64$ relative to PI, using one quarter as many stored filter coefficients. Increasing Q from 16 to 64 provides a further 3.7% MSE reduction. This comparison quantifies the storage tradeoff within the evaluated bank family; the gap to continuous adaptation is assessed separately below.

At $Q = 16$, validation selects one timing bin and sixteen posterior-frequency bins, with routing coordinate $400^2 \widehat{f}/(400^2 + \sigma_f^2)$ in Hz. This selected router uses frequency confidence but not timing confidence. The richer routing family reduces validation MSE from 0.15130 to 0.13902 relative to raw-estimate routing. Timing resolution first appears at $Q = 32$ in this sweep.

To isolate the coefficient-design gain, we compare two banks with the same $Q = 16$ partition, thresholds, routing rule, storage, and online cost. The shared partition is selected using conditional-bank validation MSE; only the stored coefficients differ. The comparison bank replaces each conditional-moment filter with a conventional WLTV-MMSE filter synthesized at a representative point state. For cell j, this state is the empirical mean of the posterior-mean timing and frequency coordinates of the development samples routed to that cell. Neither test labels nor true test states are used.

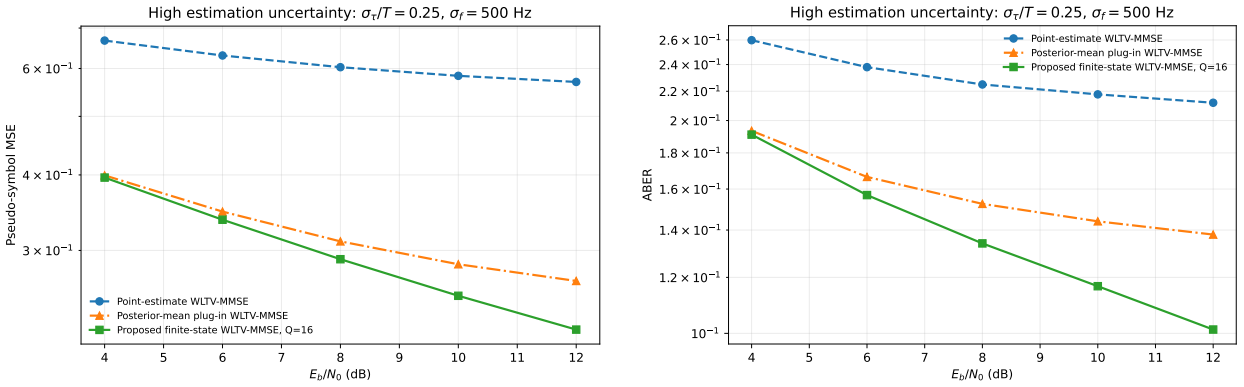
On the same high-uncertainty reference test at $E_b/N_0 = 8$ dB, the representative-state bank attains pseudo-symbol MSE 0.32286 and full-waveform ABER 0.15884. The conditional-moment bank attains 0.29013 and 0.13404, corresponding to reductions of 10.1% and 15.6%, respectively. Paired cluster-bootstrap 95% intervals for the absolute improvements are $[0.02541, 0.04065]$ and $[0.01919, 0.03075]$. Under the shared partition, this comparison isolates the benefit of designing coefficients from the conditional uncertainty distribution rather than from representative point states.

C. Timing–Frequency Uncertainty Plane

At $E_b/N_0 = 10$ dB, a 13×13 grid covers

$$0.02 \le \sigma_\tau/T \le 0.35, \qquad 25 \le \sigma_f \le 600 \text{ Hz}, \tag{68}$$

with the physical-state distribution unchanged. Each point uses 24 clusters and 500 contexts per cluster. True



(a) **(b)**

Fig. 2. Performance under high synchronization-estimation uncertainty $(\sigma_\tau/T, \sigma_f) = (0.25, 500\ \text{Hz})$. (a) Pseudo-symbol MSE. (b) Full-CPM ABER. The posterior-mean substitution receiver uses the same uncertainty information as the proposed method. The comparison quantifies the additional empirical gain of the selected conditional-moment filter bank over this baseline.

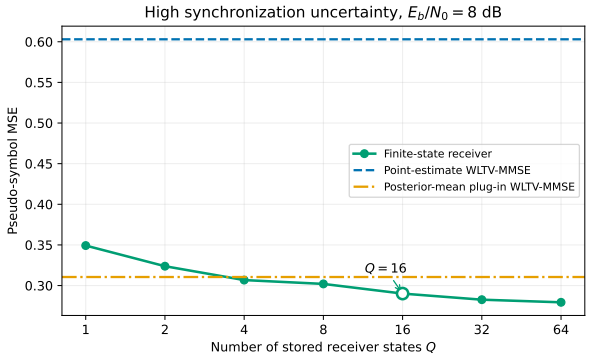


Fig. 3. Pseudo-symbol MSE versus the number Q of stored receiver states at $E_b/N_0 = 8$ dB under high synchronization-estimation uncertainty $(\sigma_\tau/T, \sigma_f) = (0.25, 500\ \text{Hz})$. The horizontal lines show the point-estimate and posterior-mean substitution WLTV-MMSE baselines. The highlighted $Q = 16$ point is the operating point used in the SNR and uncertainty-plane experiments.

states, standardized estimation errors, data, and noise are reused across grid points. For the ABER surface ratios only, the error rate is regularized to $(e + 1/2)/(12000 + 1)$, where e is the error count.

Figure 4 shows the complete evaluated domain, including regions of negative gain. MSE and ABER improve over PI at 79.9% and 87.0% of sampled points, respectively, and both improve at 79.3%. In the region $\sigma_\tau/T \geq 0.08$ and $\sigma_f \geq 200$ Hz, both metrics improve at every sampled point. Within this region, mean reductions are 47.9% and 49.5% relative to PI, and 5.7% and 16.0% relative to PM, for MSE and ABER, respectively. Large negative relative gains at low uncertainty can reflect small baseline error rates.

TABLE I

CHANNEL-ENSEMBLE REDUCTIONS RELATIVE TO PM AT $E_b/N_0 = 8$ DB, $t_0 = 300\ \mu$S, AND HIGH UNCERTAINTY. EACH STRATUM CONTAINS SIX CHANNELS; GAINS ARE COMPUTED FROM RATIOS OF AVERAGED ERRORS.

K_c (dB)	MSE reduction (%)	ABER reduction (%)
6	5.08	11.79
15	5.30	13.63
29	5.52	13.43
All eighteen	5.30	12.93

D. Channel, Age, and Calibration Sensitivity

We generate eighteen synthetic three-path channels, with six channels for each dominant-to-remaining-path power ratio $K_c \in \{6, 15, 29\}$ dB. Powers remain proportional to $(10^{K_c/10}, 0.75, 0.25)$. The two nonzero delays are sorted independent uniform draws on $[0, 7]\ \mu$s, path Doppler shifts are independent uniform draws on $[-1520, 1520]$ Hz, and non-dominant phases are independent uniform draws on $[-\pi, \pi]$, with the dominant phase set to zero. Each channel is known, remains fixed during its test, and has its own trained and validated bank. This experiment evaluates performance across channel conditions using individually fitted banks.

Both metrics improve for each of the eighteen channels; Table I summarizes the gains by power-ratio stratum. Aggregate pseudo-symbol MSE decreases from 0.28399 for PM to 0.26895 for the bank, while ABER decreases from 0.12824 to 0.11166. Stratified channel-bootstrap 95% intervals for the relative reductions are $[4.53, 6.06]\%$ and $[11.04, 14.45]\%$, respectively. Full-CPM MSE decreases from 0.28586 to 0.27096, a reduction of 5.21%. These intervals describe the synthetic channel ensemble conditional on the fitted banks.

For the reference channel, we next vary $t_0 \in \{0, 75, 150, 300, 600, 1200\}\ \mu$s, refitting the bank at each

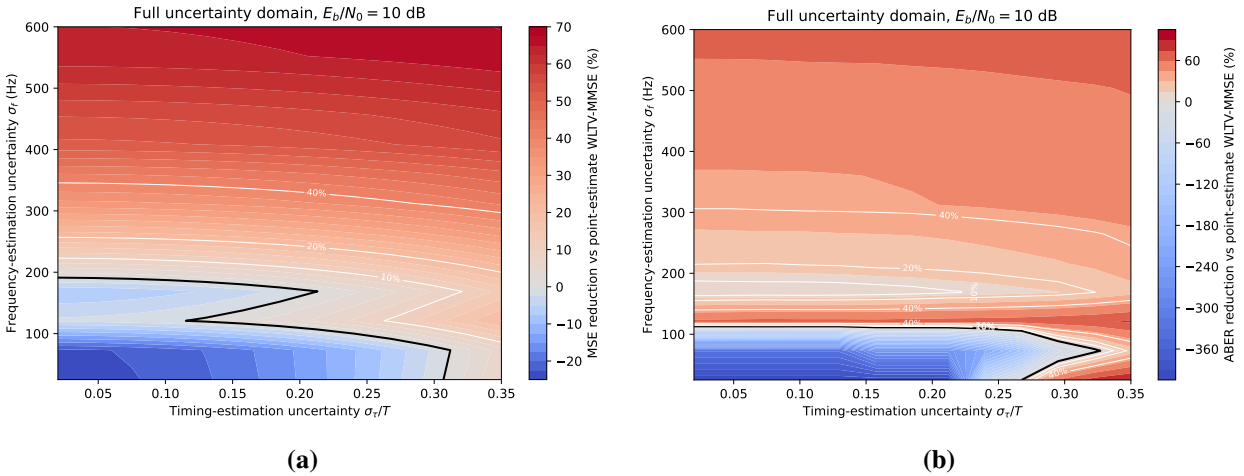


Fig. 4. Synchronization-estimation uncertainty over the evaluated domain at $E_b/N_0 = 10$ dB. (a) Relative MSE reduction and (b) relative full-CPM ABER reduction of the proposed $Q = 16$ receiver with respect to point-estimate WLTV-MMSE. The black contour denotes zero gain; warm regions favor the proposed receiver and cool regions favor point-estimate substitution.

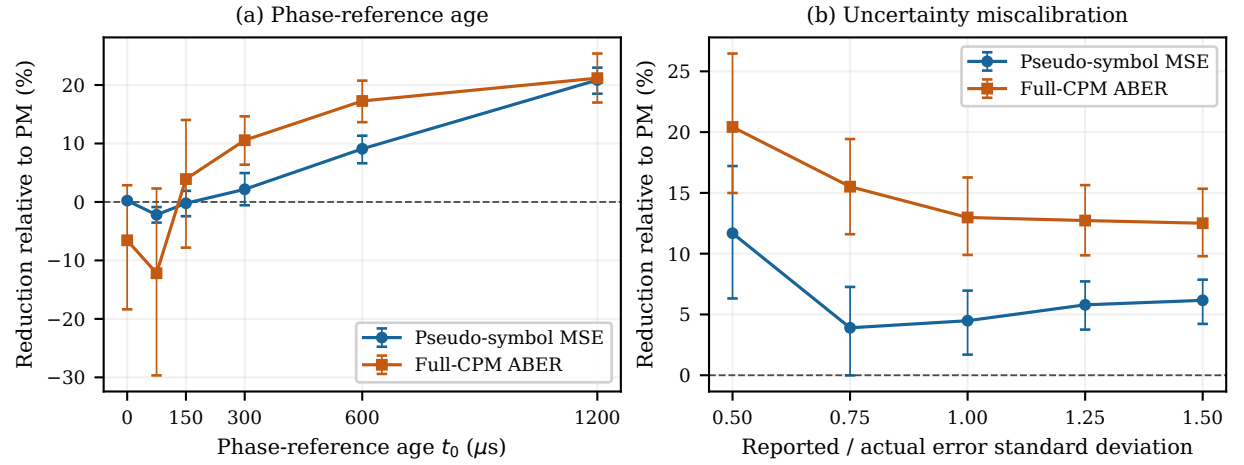


Fig. 5. Robustness tests at $E_b/N_0 = 8$ dB relative to PM. Error bars are paired cluster-bootstrap 95% intervals. (a) Reference-channel phase-reference-age sweep, with a separately fitted bank at each age and common test draws. (b) Fixed reference-channel bank with both reported error standard deviations multiplied by c, while actual errors remain unchanged. Positive values favor the bank; all predefined conditions are shown.

phase-reference age. Figure 5(a) shows how the benefit of finite-state adaptation depends on this age. At 75 μs, MSE and ABER increase by 2.2% and 12.2%, respectively, relative to PM. At 150 μs, the MSE difference is inconclusive. The independent test ensemble at 300 μs gives a 2.2% MSE reduction, with a confidence interval that includes zero. At 600 and 1200 μs, relative MSE reductions increase to 9.1% and 20.9%, respectively, although absolute errors also increase. At 1200 μs, the bank MSE is 1.08684, exceeding the zero-estimate MSE of one. These results show that relative gains must be interpreted alongside absolute error levels as the phase reference ages.

For calibration sensitivity, the actual error standard deviations remain $(0.25T, 500$ Hz$)$, while the receiver is given $(c\,0.25T, c\,500$ Hz$)$, with $c \in \{0.5, 0.75, 1, 1.25, 1.5\}$. The bank and thresholds remain fixed; only the reported-confidence routing feature changes. PM uses the same reported values. Figure 5(b) shows positive mean MSE and ABER gains at every tested c. MSE reductions range from 3.9% to 11.7%, and ABER reductions range from 12.5% to 20.4%. The MSE interval at $c = 0.75$ includes zero. For the two largest values of c, the reported frequency uncertainty also exceeds the training range. These results quantify sensitivity to the tested multiplicative miscalibration.

TABLE II
INDEPENDENT REFERENCE TEST. CONDITIONAL MODEL MSE AVERAGES POSTERIOR-INTEGRATED RISKS OVER SIDE INFORMATION; FULL-CPM QUANTITIES USE SAMPLED PHYSICAL STATES AND WAVEFORMS.

Receiver	Conditional model MSE	Full-CPM MSE	Full-CPM ABER
PI	0.62485	0.59612	0.23425
PM	0.27223	0.25671	0.09896
Bank, $Q = 16$	0.25767	0.24397	0.08511
Continuous	0.23590	0.22657	0.06670
Matched/oracle	0.07804	0.08104	0.00084

TABLE III
SINGLE-THREAD PYTHON CPU TIMINGS PER WINDOW. MEDIANS AND 10TH–90TH PERCENTILES ARE COMPUTED OVER 41 RANDOMLY INTERLEAVED BLOCKS OF 128 CALLS. FRONT-END PROCESSING AND BIT DECISIONS ARE EXCLUDED.

Operation	Median (μs)	10th–90th (μs)
Routing only	2.95	2.86–3.27
Filter only	1.77	1.72–2.62
Routing + filter	4.30	4.03–5.05
PI, dense	395.75	376.47–479.25
PM, dense	396.26	378.78–456.02
PI, 18-column form	376.28	356.78–449.85
PM, 18-column form	374.03	360.80–437.61

E. Numerical Continuous-Adaptation Reference

On an independent 256-cluster reference-channel test at $E_b/N_0 = 8$ dB, we numerically integrate the Gaussian posterior of $(\tau/T, f)$ conditioned on each complete side-information realization. Tensor Gauss–Hermite quadrature with 40 nodes per coordinate provides the conditional real moments used to construct the affine-WL reference of Theorem 2. Using 24 nodes per coordinate changes the per-realization conditional risk by at most 1.64×10^{-7}. The resulting filters incur at most 5.27×10^{-12} additional risk when evaluated using the finer quadrature. These numerical convergence checks do not constitute rigorous integration-error bounds.

Table II distinguishes posterior-integrated model risks from empirical full-waveform results. These quantities can differ because of both the waveform model and finite sampling. The matched-state/oracle receiver uses true synchronization; its integrated risk averages the matched-state MMSE over each posterior. For the dominant-component model, the conditional-risk averages give

$$\mathcal{G}_{\mathrm{PI}} \simeq 0.38895, \qquad \mathcal{G}_{\mathrm{info}} \simeq 0.15786,$$
$$\mathcal{J}_{\mathrm{bank}} - \mathcal{J}_{\mathsf{S}}^{\star} \simeq 0.02176.$$

All values are per target coordinate. The bank's excess risk has a paired 95% interval of $[0.02006, 0.02369]$, equals 9.2% of the continuous-reference risk, and agrees with the quadratic excess-risk identity to 1.23×10^{-15}.

This excess risk includes the implemented bank's partition restrictions and moment-estimation error; it is not the minimum population compression penalty. The continuous reference attains full-CPM MSE and ABER of 0.22657 and 0.06670, compared with 0.24397 and 0.08511 for the bank. The comparison quantifies the remaining performance gain available through continuous adaptation, whose online computational cost must also be considered.

V. DISCUSSION AND DESIGN IMPLICATIONS

For the same target, observation model, and side information, an admissible implemented bank satisfies

$$\mathcal{J}_{\mathrm{PI}} - \mathcal{J}_{\mathrm{bank}} = \mathcal{G}_{\mathrm{PI}} - \left(\mathcal{J}_{\mathrm{bank}} - \mathcal{J}_{\mathsf{S}}^{\star}\right). \tag{69}$$

Thus, strict MSE improvement occurs precisely when $\mathcal{J}_{\mathrm{bank}} - \mathcal{J}_{\mathsf{S}}^{\star} < \mathcal{G}_{\mathrm{PI}}$. In practical terms, the benefit of accounting for physical-state uncertainty must exceed the loss incurred by the implemented finite-state approximation.

The reference experiment at $E_b/N_0 = 8$ dB demonstrates this regime: the sixteen-state bank reduces pseudo-symbol MSE by 51.9% relative to point-estimate WLTV-MMSE and by 6.6% relative to posterior-mean substitution. In the uncertainty plane sampled at $E_b/N_0 = 10$ dB, both MSE and ABER improve over point-estimate adaptation at every tested point satisfying $\sigma_\tau/T \geq 0.08$ and $\sigma_f \geq 200$ Hz.

For the implemented zero-mean receiver, applying a 64×2 filter requires 128 real multiplications and 126 additions per two-target window. A $Q = 16$ bank stores 2048 real coefficients (16 KiB in 64-bit precision), plus 15 thresholds. After feature computation, binary-search frequency routing requires at most four comparisons. These counts exclude common sampling, synchronization, and bit decisions. Changes in the channel, phase-reference age, or noise level require appropriate bank updates.

Table III uses one thread on an AMD EPYC 9V74 CPU with Python 3.12.14, NumPy 2.3.5, and SciPy 1.17.0, including Python call and loop overhead. Plug-in timings include channel/moment formation, Cholesky factorization, and filter application. Besides the dense 64×64 solve, an equivalent implementation exploits $\mathbf{B}$'s 18 columns:

$$\mathbf{W} = \mathbf{B}(\mathbf{B}^T\mathbf{B} + n_r\mathbf{I}_{18})^{-1}\mathbf{E},$$

where $\mathbf{E}$ selects the two target coordinates. The implementations agree within 1.7×10^{-15} in output. Median routing-plus-application time is 4.30 μs, versus 374.03 μs for the faster measured PM implementation: an approximately 87-fold reduction with PM synthesis performed every window.

A conditional-moment refresh using 6000 development states and the fixed selected partition takes a median 1.64 s over seven runs; partition reselection is additional. Updating only the noise variance and refactoring

sixteen stored moment matrices takes 0.42 ms. Against PM synthesis once per window, these costs are amortized after approximately 4430 and 2 windows, respectively. These are software measurements, not embedded-device latency or energy guarantees. Less frequent plug-in adaptation reduces the savings; rapidly changing conditions can make refresh cost dominant.

The adaptation complements low-complexity WL and banded structures [1], [8], [10] and partitioned turbo equalization [11], [12]. The matched-budget experiment isolates conditional-moment design gains with partition, storage, and routing fixed; it does not reproduce complete published receivers. Unknown or drifting channels, non-Gaussian estimation errors, training variability, and embedded implementation require further evaluation. The architecture is most useful when uncertainty-aware design improves accuracy, memory accommodates the bank, and conditions persist long enough to amortize refresh.

VI. Conclusion

We developed finite-state, uncertainty-aware WL equalization for aeronautical GMSK links with limited onboard computation and memory. Synchronization estimates and reliability information select stored filters computed from conditional physical-state moments. Exact excess-MSE identities, a design–information loss decomposition, and local mismatch certificates characterize adaptation accuracy and robustness.

On the reference channel at $E_b/N_0 = 8$ dB under high synchronization-estimation uncertainty, the $Q = 16$ bank reduces pseudo-symbol MSE by 51.9% relative to point-estimate WLTV-MMSE and by 6.6% relative to posterior-mean substitution.

The bank stores 2048 real coefficients and replaces repeated online synthesis with filter selection and application. It improves on point-estimate adaptation when its excess risk relative to continuous conditional adaptation is smaller than the plug-in design loss. The measured online and refresh costs support its use when side information enables accurate filter selection and operating conditions persist long enough to amortize bank updates.

Acknowledgment

OpenAI's ChatGPT assisted with language editing, organization, and LaTeX presentation of the manuscript, and with clarifying explanations and intermediate derivations in the supplementary appendices. The authors retain responsibility for the final content and its verification.

References

[1] D. Darsena, G. Gelli, I. Iudice, and F. Verde, "Equalization techniques of control and non-payload communication links for unmanned aerial vehicles," *IEEE Access*, vol. 6, pp. 4485–4496, 2018.

[2] K. Murota and K. Hirade, "GMSK modulation for digital mobile radio telephony," *IEEE Transactions on Communications*, vol. 29, no. 7, pp. 1044–1050, Jul. 1981.

[3] P. A. Laurent, "Exact and approximate construction of digital phase modulations by superposition of amplitude modulated pulses (AMP)," *IEEE Transactions on Communications*, vol. 34, no. 2, pp. 150–160, Feb. 1986.

[4] B. Picinbono and P. Chevalier, "Widely linear estimation with complex data," *IEEE Transactions on Signal Processing*, vol. 43, no. 8, pp. 2030–2033, Aug. 1995.

[5] W. H. Gerstacker, R. Schober, and A. Lampe, "Receivers with widely linear processing for frequency-selective channels," *IEEE Transactions on Communications*, vol. 51, no. 9, pp. 1512–1523, Sep. 2003.

[6] D. Darsena, G. Gelli, I. Iudice, and F. Verde, "Second-order statistics of one-sided CPM signals," *IEEE Signal Processing Letters*, vol. 24, no. 10, pp. 1512–1516, Oct. 2017.

[7] P. Chevalier, J.-P. Delmas, and R. Lamberti, "New insights into widely linear MMSE receivers for communication networks using data-like rectilinear or quasi-rectilinear signals," *IEEE Transactions on Signal Processing*, vol. 72, pp. 5156–5173, 2024.

[8] J. Chae, J. Choi, J. Kim, and J. H. Cho, "A low-complexity widely-linear MMSE equalizer for DFT-spread OFDM with frequency-domain spectrum shaping," *IEEE Transactions on Wireless Communications*, vol. 23, no. 4, pp. 3465–3479, 2023.

[9] Y. Luo *et al.*, "Widely linear augmented extreme learning machine based impairments compensation for satellite communications," *IEEE Transactions on Vehicular Technology*, vol. 74, no. 11, pp. 17 725–17 737, 2025.

[10] R. Chayot *et al.*, "A frequency-domain band-MMSE equalizer for continuous phase modulation over frequency-selective time-varying channels," in *Proc. 26th European Signal Processing Conference (EUSIPCO)*, 2018, pp. 932–936.

[11] K. Kim, N. Kalantarova, S. S. Kozat, and A. C. Singer, "Linear MMSE-optimal turbo equalization using context trees," *IEEE Transactions on Signal Processing*, vol. 61, no. 12, pp. 3041–3055, Jun. 2013.

[12] K. Kim, J. W. Choi, S. S. Kozat, and A. C. Singer, "Low complexity turbo-equalization: A clustering approach," *IEEE Communications Letters*, vol. 18, no. 6, pp. 1063–1066, Jun. 2014.

[13] L. Salamanca, J. J. Murillo-Fuentes, and F. Pérez-Cruz, "Bayesian equalization for LDPC channel decoding," *IEEE Transactions on Signal Processing*, vol. 60, no. 5, pp. 2672–2676, May 2012.

[14] R. Boloix-Tortosa and J. J. Murillo-Fuentes, "Complex Gaussian processes for regression and their connection to WLMMSE," *IEEE Signal Processing Letters*, vol. 32, pp. 386–390, 2024.

[15] N. Shlezinger, Y. C. Eldar, and M. R. D. Rodrigues, "Hardware-limited task-based quantization," *IEEE Transactions on Signal Processing*, vol. 67, no. 20, pp. 5223–5238, Oct. 2019.

[16] P. A. Bello, "Characterization of randomly time-variant linear channels," *IEEE Transactions on Communication Systems*, vol. 11, no. 4, pp. 360–393, Dec. 1963.

[17] P. J. Schreier and L. L. Scharf, *Statistical Signal Processing of Complex-Valued Data: The Theory of Improper and Noncircular Signals*. Cambridge, U.K.: Cambridge University Press, 2010.

[18] S. M. Kay, *Fundamentals of Statistical Signal Processing: Estimation Theory*. Englewood Cliffs, NJ, USA: Prentice Hall, 1993, vol. 1.

[19] S. P. Lloyd, "Least squares quantization in PCM," *IEEE Transactions on Information Theory*, vol. 28, no. 2, pp. 129–137, Mar. 1982.

[20] Y. Linde, A. Buzo, and R. M. Gray, "An algorithm for vector quantizer design," *IEEE Transactions on Communications*, vol. 28, no. 1, pp. 84–95, Jan. 1980.

Supplementary material: derivations and proofs

APPENDIX A
SYNCHRONIZATION-DERIVATIVE FORMULAS

Throughout this appendix, the receiver coefficients $(\mathbf{a}, \mathbf{W})$ and the physical quantities $\boldsymbol{\xi} = (\mathbf{h}, \mathbf{R}_n^{\mathrm{true}})$ are held fixed. Subscripts $q, r \in \{\tau, \nu\}$ denote partial derivatives with respect to the normalized synchronization coordinates ϵ_τ and ϵ_ν, respectively. All state-dependent quantities are evaluated at the same $(\boldsymbol{\epsilon}, \boldsymbol{\xi})$. The formulas below assume that the effective pulses possess the required derivatives.

Recall that $\eta = T_s/T$ and

$$\mathbf{D} = \mathrm{diag}(t_0/T_s, t_0/T_s + 1, \ldots, t_0/T_s + N - 1).$$

The first-order channel derivatives are given in (37). The corresponding mean and cross-covariance derivatives are

$$\boldsymbol{\mu}_{y,q} = \begin{bmatrix} \mathbf{H}_q \boldsymbol{\mu}_b \\ \mathbf{H}_q^* \boldsymbol{\mu}_b^* \end{bmatrix}, \qquad \mathbf{C}_q = \begin{bmatrix} \mathbf{H}_q \mathbf{R}_b \\ \mathbf{H}_q^* \mathbf{C}_b^* \end{bmatrix}.$$

Writing

$$\mathbf{R}_y = \begin{bmatrix} \mathbf{P} & \mathbf{Q} \\ \mathbf{Q}^* & \mathbf{P}^* \end{bmatrix},$$

with $\mathbf{P} = \mathbf{H}\mathbf{R}_b\mathbf{H}^H + \mathbf{R}_n^{\mathrm{true}}$ and $\mathbf{Q} = \mathbf{H}\mathbf{C}_b\mathbf{H}^T$, we obtain

$$\begin{aligned} \mathbf{P}_q &= \mathbf{H}_q\mathbf{R}_b\mathbf{H}^H + \mathbf{H}\mathbf{R}_b\mathbf{H}_q^H, \\ \mathbf{Q}_q &= \mathbf{H}_q\mathbf{C}_b\mathbf{H}^T + \mathbf{H}\mathbf{C}_b\mathbf{H}_q^T. \end{aligned}$$

There is no noise-covariance derivative because $\mathbf{R}_n^{\mathrm{true}}$ is held fixed.

The second-order channel derivatives satisfy

$$\mathbf{H}_{\tau\nu} = \mathbf{H}_{\nu\tau} = j2\pi\eta\mathbf{D}\mathbf{H}_\tau, \qquad \mathbf{H}_{\nu\nu} = -(2\pi\eta)^2\mathbf{D}^2\mathbf{H}.$$

The entries of $\mathbf{H}_{\tau\tau}$ are obtained from those of $\mathbf{H}_\tau$ by replacing $-T\phi_k'(\cdot)$ with $T^2\phi_k''(\cdot)$. Consequently,

$$\boldsymbol{\mu}_{y,qr} = \begin{bmatrix} \mathbf{H}_{qr} \boldsymbol{\mu}_b \\ \mathbf{H}_{qr}^* \boldsymbol{\mu}_b^* \end{bmatrix}, \qquad \mathbf{C}_{qr} = \begin{bmatrix} \mathbf{H}_{qr} \mathbf{R}_b \\ \mathbf{H}_{qr}^* \mathbf{C}_b^* \end{bmatrix}.$$

Applying the product rule gives

$$\begin{aligned} \mathbf{P}_{qr} &= \mathbf{H}_{qr}\mathbf{R}_b\mathbf{H}^H + \mathbf{H}_q\mathbf{R}_b\mathbf{H}_r^H \\ &\quad + \mathbf{H}_r\mathbf{R}_b\mathbf{H}_q^H + \mathbf{H}\mathbf{R}_b\mathbf{H}_{qr}^H, \\ \mathbf{Q}_{qr} &= \mathbf{H}_{qr}\mathbf{C}_b\mathbf{H}^T + \mathbf{H}_q\mathbf{C}_b\mathbf{H}_r^T \\ &\quad + \mathbf{H}_r\mathbf{C}_b\mathbf{H}_q^T + \mathbf{H}\mathbf{C}_b\mathbf{H}_{qr}^T. \end{aligned}$$

Since the differentiation variables are real, differentiation commutes with complex conjugation. Thus,

$$\mathbf{R}_{y,q} = \begin{bmatrix} \mathbf{P}_q & \mathbf{Q}_q \\ \mathbf{Q}_q^* & \mathbf{P}_q^* \end{bmatrix}, \qquad \mathbf{R}_{y,qr} = \begin{bmatrix} \mathbf{P}_{qr} & \mathbf{Q}_{qr} \\ \mathbf{Q}_{qr}^* & \mathbf{P}_{qr}^* \end{bmatrix}.$$

For a frozen affine receiver $\mathcal{R} = (\mathbf{a}, \mathbf{W})$, let

$$\mathbf{m}_{\mathcal{R}} = \boldsymbol{\mu}_b - \mathbf{a} - \mathbf{W}^H\boldsymbol{\mu}_y.$$

Because the coefficients are fixed, $\mathbf{m}_{\mathcal{R},q} = -\mathbf{W}^H\boldsymbol{\mu}_{y,q}$. Differentiating (38) therefore gives

$$\begin{aligned} M_{\mathcal{R},q} &= -2\Re\{\mathbf{m}_{\mathcal{R}}^H\mathbf{W}^H\boldsymbol{\mu}_{y,q}\} \\ &\quad - 2\Re\{\mathrm{tr}(\mathbf{W}^H\mathbf{C}_q)\} + \mathrm{tr}(\mathbf{W}^H\mathbf{R}_{y,q}\mathbf{W}), \end{aligned} \tag{70}$$

$$\begin{aligned} M_{\mathcal{R},qr} &= 2\Re\{\boldsymbol{\mu}_{y,r}^H\mathbf{W}\mathbf{W}^H\boldsymbol{\mu}_{y,q} - \mathbf{m}_{\mathcal{R}}^H\mathbf{W}^H\boldsymbol{\mu}_{y,qr}\} \\ &\quad - 2\Re\{\mathrm{tr}(\mathbf{W}^H\mathbf{C}_{qr})\} + \mathrm{tr}(\mathbf{W}^H\mathbf{R}_{y,qr}\mathbf{W}). \end{aligned} \tag{71}$$

The gradient of $D_s(\boldsymbol{\epsilon}; \boldsymbol{\xi})$ is obtained by subtracting the reference-receiver first derivatives from the plug-in WLTV first derivatives. The Hessian is obtained by the same subtraction of second derivatives. Evaluating these expressions at $\boldsymbol{\epsilon}_0$ gives $\mathbf{g}_s$ and $\mathbf{B}_s$.

APPENDIX B
PROOF OF LEMMA 1

Recall the observation model $\mathbf{y} = \mathbf{H}(\boldsymbol{\theta})\mathbf{b} + \mathbf{n}$, where $\mathbf{H}(\boldsymbol{\theta}) \equiv \mathbf{H}(\boldsymbol{\epsilon}, \mathbf{h})$. Under A1–A2, $\mathbb{E}[\mathbf{b} \mid \boldsymbol{\theta}, \mathsf{S}] = \boldsymbol{\mu}_b$ and $\mathbb{E}[\mathbf{n} \mid \boldsymbol{\theta}, \mathsf{S}] = \mathbf{0}$. Hence,

$$\mathbb{E}[\underline{\mathbf{y}} \mid \boldsymbol{\theta}, \mathsf{S}] = \begin{bmatrix} \mathbf{H}(\boldsymbol{\theta})\boldsymbol{\mu}_b \\ \mathbf{H}(\boldsymbol{\theta})^*\boldsymbol{\mu}_b^* \end{bmatrix} = \boldsymbol{\mu}_y(\boldsymbol{\theta}).$$

The tower property gives $\boldsymbol{\mu}_{\mathsf{S}} = \mathbb{E}[\boldsymbol{\mu}_y(\boldsymbol{\theta}) \mid \mathsf{S}]$.

For the cross-covariance, decompose

$$\underline{\mathbf{y}} - \boldsymbol{\mu}_{\mathsf{S}} = \big(\underline{\mathbf{y}} - \boldsymbol{\mu}_y(\boldsymbol{\theta})\big) + \big(\boldsymbol{\mu}_y(\boldsymbol{\theta}) - \boldsymbol{\mu}_{\mathsf{S}}\big).$$

Substitution into the definition of $\mathbf{C}_{\mathsf{S}}$ yields

$$\begin{aligned} \mathbf{C}_{\mathsf{S}} &= \mathbb{E}\big[(\underline{\mathbf{y}} - \boldsymbol{\mu}_y(\boldsymbol{\theta}))(\mathbf{b} - \boldsymbol{\mu}_b)^H \mid \mathsf{S}\big] \\ &\quad + \mathbb{E}\big[(\boldsymbol{\mu}_y(\boldsymbol{\theta}) - \boldsymbol{\mu}_{\mathsf{S}})(\mathbf{b} - \boldsymbol{\mu}_b)^H \mid \mathsf{S}\big]. \end{aligned}$$

The second term vanishes because $\boldsymbol{\mu}_y(\boldsymbol{\theta}) - \boldsymbol{\mu}_{\mathsf{S}}$ is $(\boldsymbol{\theta}, \mathsf{S})$-measurable and A1 gives $\mathbb{E}[\mathbf{b} - \boldsymbol{\mu}_b \mid \boldsymbol{\theta}, \mathsf{S}] = \mathbf{0}$.

For the first term, A1–A2 imply

$$\mathbb{E}\big[(\underline{\mathbf{y}} - \boldsymbol{\mu}_y(\boldsymbol{\theta}))(\mathbf{b} - \boldsymbol{\mu}_b)^H \mid \boldsymbol{\theta}, \mathsf{S}\big] = \mathbf{C}(\boldsymbol{\theta}).$$

Applying the tower property therefore gives $\mathbf{C}_{\mathsf{S}} = \mathbb{E}[\mathbf{C}(\boldsymbol{\theta}) \mid \mathsf{S}]$.

The conditional law of total covariance gives

$$\begin{aligned} \mathbf{R}_{\mathsf{S}} &= \mathbb{E}\big[\mathrm{Cov}(\underline{\mathbf{y}} \mid \boldsymbol{\theta}, \mathsf{S}) \mid \mathsf{S}\big] \\ &\quad + \mathrm{Cov}\left(\mathbb{E}[\underline{\mathbf{y}} \mid \boldsymbol{\theta}, \mathsf{S}] \mid \mathsf{S}\right). \end{aligned}$$

Under A1–A2, $\mathrm{Cov}(\underline{\mathbf{y}} \mid \boldsymbol{\theta}, \mathsf{S}) = \mathbf{R}_y(\boldsymbol{\theta})$. Together with the conditional-mean identity above, this proves (34).

To establish the lower bound, let $\underline{\mathbf{n}} = [\,\mathbf{n}^T \;\; \mathbf{n}^H\,]^T$. Properness under A2 gives the conditional augmented noise covariance

$$\mathbf{R}_{\underline{n}}(\boldsymbol{\theta}) = \begin{bmatrix} \mathbf{R}_n^{\mathrm{true}} & \mathbf{0} \\ \mathbf{0} & (\mathbf{R}_n^{\mathrm{true}})^* \end{bmatrix}.$$

By A3, $\mathbf{R}_{\underline{n}}(\boldsymbol{\theta}) \succeq \sigma_0^2 \mathbf{I}_{2N}$. The signal covariance is positive semidefinite, and the augmented signal and noise are uncorrelated under A2. Thus,

$$\mathbf{R}_y(\boldsymbol{\theta}) \succeq \mathbf{R}_{\underline{n}}(\boldsymbol{\theta}) \succeq \sigma_0^2 \mathbf{I}_{2N} \qquad \text{almost surely.}$$

Conditional expectation preserves this ordering. Since $\mathrm{Cov}(\boldsymbol{\mu}_y(\boldsymbol{\theta}) \mid \mathsf{S}) \succeq \mathbf{0}$, (34) implies

$$\mathbf{R}_{\mathsf{S}} \succeq \sigma_0^2 \mathbf{I}_{2N} \qquad \text{almost surely.}$$

This completes the proof.

Appendix C
Proof of Lemma 2

Condition on U throughout and suppress the explicit U-dependence of $\mathbf{a}$ and $\mathbf{W}$. Define

$$\widetilde{\mathbf{b}} = \mathbf{b} - \boldsymbol{\mu}_b, \qquad \widetilde{\mathbf{y}} = \underline{\mathbf{y}} - \boldsymbol{\mu}_U.$$

Both variables have zero conditional mean, with

$$\begin{aligned}
\mathbb{E}[\widetilde{\mathbf{b}}\widetilde{\mathbf{b}}^H \mid U] &= \mathbf{R}_b, \\
\mathbb{E}[\widetilde{\mathbf{y}}\widetilde{\mathbf{y}}^H \mid U] &= \mathbf{R}_U, \\
\mathbb{E}[\widetilde{\mathbf{y}}\widetilde{\mathbf{b}}^H \mid U] &= \mathbf{C}_U.
\end{aligned}$$

Let $\mathbf{d}_U = \boldsymbol{\mu}_b - \mathbf{a} - \mathbf{W}^H \boldsymbol{\mu}_U$. The estimation error is

$$\mathbf{b} - \mathbf{a} - \mathbf{W}^H \underline{\mathbf{y}} = \mathbf{d}_U + \widetilde{\mathbf{b}} - \mathbf{W}^H \widetilde{\mathbf{y}}.$$

The cross term between $\mathbf{d}_U$ and the centered error has zero conditional expectation. Consequently,

$$\mathcal{J}(\mathbf{a}, \mathbf{W} \mid U) = \|\mathbf{d}_U\|_2^2 + \mathbb{E}\Big[\|\widetilde{\mathbf{b}} - \mathbf{W}^H \widetilde{\mathbf{y}}\|_2^2 \mid U\Big].$$

Expanding the second term gives

$$\mathbb{E}[\|\widetilde{\mathbf{b}}\|_2^2 \mid U] = \mathrm{tr}(\mathbf{R}_b)$$

and

$$\mathbb{E}[\|\mathbf{W}^H \widetilde{\mathbf{y}}\|_2^2 \mid U] = \mathrm{tr}(\mathbf{W}^H \mathbf{R}_U \mathbf{W}).$$

Using the trace identity for a scalar product,

$$\mathbb{E}[\widetilde{\mathbf{b}}^H \mathbf{W}^H \widetilde{\mathbf{y}} \mid U] = \mathrm{tr}(\mathbf{W}^H \mathbf{C}_U).$$

The two conjugate cross terms therefore sum to $-2\Re\{\mathrm{tr}(\mathbf{W}^H \mathbf{C}_U)\}$, proving (35).

For fixed $\mathbf{W}$, the only term depending on $\mathbf{a}$ is $\|\boldsymbol{\mu}_b - \mathbf{a} - \mathbf{W}^H \boldsymbol{\mu}_U\|_2^2$. Its minimum is zero, attained uniquely at $\mathbf{a} = \boldsymbol{\mu}_b - \mathbf{W}^H \boldsymbol{\mu}_U$.

Appendix D
Proof of Theorem 1

Fix s and $\boldsymbol{\xi}$. The receivers $\mathcal{R}_{\mathrm{PI}}$ and $\mathcal{R}_{\mathrm{r}}$ remain unchanged as $\boldsymbol{\epsilon}$ varies, so D_s depends on $\boldsymbol{\epsilon}$ only through the physical-state statistics.

By the assumed continuous differentiability, Taylor expansion around $\boldsymbol{\epsilon}_0$ gives

$$\begin{aligned}
D_s(\boldsymbol{\epsilon}_0 + \boldsymbol{\delta}; \boldsymbol{\xi}) = D_s(\boldsymbol{\epsilon}_0; \boldsymbol{\xi}) + \nabla_{\boldsymbol{\epsilon}} D_s(\boldsymbol{\epsilon}_0; \boldsymbol{\xi})^T \boldsymbol{\delta} \\
+ \frac{1}{2} \boldsymbol{\delta}^T \nabla_{\boldsymbol{\epsilon}}^2 D_s(\boldsymbol{\epsilon}_0; \boldsymbol{\xi}) \boldsymbol{\delta} + R_3(\boldsymbol{\delta}).
\end{aligned}$$

Substituting the definitions of Γ_s, $\mathbf{g}_s$, and $\mathbf{B}_s$ proves (39). Since $\Gamma_s > 0$, the expansion point satisfies $D_s(\boldsymbol{\epsilon}_0; \boldsymbol{\xi}) < 0$ and is therefore viable.

For $\boldsymbol{\delta} \in \mathcal{B}_r$, the segment from $\boldsymbol{\epsilon}_0$ to $\boldsymbol{\epsilon}_0 + \boldsymbol{\delta}$ lies in $\boldsymbol{\epsilon}_0 + \mathcal{B}_r$. The integral form of the remainder is

$$R_3(\boldsymbol{\delta}) = \frac{1}{2} \int_0^1 (1-t)^2 \nabla_{\boldsymbol{\epsilon}}^3 D_s(\boldsymbol{\epsilon}_0 + t\boldsymbol{\delta}; \boldsymbol{\xi})[\boldsymbol{\delta}, \boldsymbol{\delta}, \boldsymbol{\delta}]\, dt.$$

The definition of $L_3(r)$ and $\frac{1}{2}\int_0^1 (1-t)^2\, dt = 1/6$ therefore give

$$|R_3(\boldsymbol{\delta})| \le \frac{L_3(r)}{6} \|\boldsymbol{\delta}\|_2^3.$$

Hence,

$$\begin{aligned}
q_s(\boldsymbol{\delta}) - \frac{L_3(r)}{6} \|\boldsymbol{\delta}\|_2^3 \le D_s(\boldsymbol{\epsilon}_0 + \boldsymbol{\delta}; \boldsymbol{\xi}), \\
D_s(\boldsymbol{\epsilon}_0 + \boldsymbol{\delta}; \boldsymbol{\xi}) \le q_s(\boldsymbol{\delta}) + \frac{L_3(r)}{6} \|\boldsymbol{\delta}\|_2^3.
\end{aligned}$$

For a point in $\mathcal{V}_{\mathrm{in}}(r)$, the upper bound is strictly negative, so the point belongs to $\mathcal{V}_s(\boldsymbol{\xi})$. Conversely, at any viable point within the ball, the lower bound is no greater than the strictly negative value of D_s. That point therefore belongs to $\mathcal{V}_{\mathrm{out}}(r)$. These two observations prove (42).

Appendix E
Proof of Theorem 2

Apply Lemma 2 with $U = \mathsf{S}$. For a given realization of S, the conditional MSE is

$$\begin{aligned}
\mathrm{tr}(\mathbf{R}_b) + \|\boldsymbol{\mu}_b - \mathbf{a} - \mathbf{W}^H \boldsymbol{\mu}_{\mathsf{S}}\|_2^2 \\
- 2\Re\{\mathrm{tr}(\mathbf{W}^H \mathbf{C}_{\mathsf{S}})\} + \mathrm{tr}(\mathbf{W}^H \mathbf{R}_{\mathsf{S}} \mathbf{W}).
\end{aligned}$$

For fixed $\mathbf{W}$, the unique minimizing offset is $\mathbf{a} = \boldsymbol{\mu}_b - \mathbf{W}^H \boldsymbol{\mu}_{\mathsf{S}}$.

Since $\mathbf{R}_{\mathsf{S}} \succ \mathbf{0}$ almost surely, the remaining quadratic expression is strictly convex in $\mathbf{W}$. Set $\mathbf{W}_\star = \mathbf{R}_{\mathsf{S}}^{-1} \mathbf{C}_{\mathsf{S}}$. Completing the square gives

$$\begin{aligned}
&\mathrm{tr}(\mathbf{W}^H \mathbf{R}_{\mathsf{S}} \mathbf{W}) - 2\Re\{\mathrm{tr}(\mathbf{W}^H \mathbf{C}_{\mathsf{S}})\} \\
&\quad = \mathrm{tr}\big((\mathbf{W} - \mathbf{W}_\star)^H \mathbf{R}_{\mathsf{S}} (\mathbf{W} - \mathbf{W}_\star)\big) \\
&\qquad - \mathrm{tr}\big(\mathbf{C}_{\mathsf{S}}^H \mathbf{R}_{\mathsf{S}}^{-1} \mathbf{C}_{\mathsf{S}}\big)\,.
\end{aligned} \tag{72}$$

The first term on the right is nonnegative and vanishes only at $\mathbf{W} = \mathbf{W}_\star$. Together with the optimal offset, this gives (45).

The conditional joint covariance satisfies

$$\begin{bmatrix} \mathbf{R}_{\mathsf{S}} & \mathbf{C}_{\mathsf{S}} \\ \mathbf{C}_{\mathsf{S}}^H & \mathbf{R}_b \end{bmatrix} \succeq \mathbf{0}.$$

Its Schur complement gives

$$\mathbf{R}_b - \mathbf{C}_{\mathsf{S}}^H \mathbf{R}_{\mathsf{S}}^{-1} \mathbf{C}_{\mathsf{S}} \succeq \mathbf{0}.$$

Therefore,

$$0 \le \operatorname{tr}\big(\mathbf{C}_{\mathsf{S}}^H \mathbf{R}_{\mathsf{S}}^{-1} \mathbf{C}_{\mathsf{S}}\big) \le \operatorname{tr}(\mathbf{R}_b) \qquad \text{almost surely.}$$

The optimal estimate can be written as

$$\widehat{\mathbf{b}}_{\mathsf{S}}^\star = \boldsymbol{\mu}_b + \mathbf{W}_\star^H (\underline{\mathbf{y}} - \boldsymbol{\mu}_{\mathsf{S}}),$$

so

$$\mathbb{E}[\|\widehat{\mathbf{b}}_{\mathsf{S}}^\star\|_2^2 \mid \mathsf{S}] = \|\boldsymbol{\mu}_b\|_2^2 + \operatorname{tr}\big(\mathbf{C}_{\mathsf{S}}^H \mathbf{R}_{\mathsf{S}}^{-1} \mathbf{C}_{\mathsf{S}}\big).$$

This is bounded by $\|\boldsymbol{\mu}_b\|_2^2 + \operatorname{tr}(\mathbf{R}_b)$, which is finite under A4. The minimizing estimate is therefore admissible. Its coefficients are measurable because conditional moments are measurable and matrix inversion is continuous on the positive-definite matrices.

The minimum conditional MSE is

$$\operatorname{tr}(\mathbf{R}_b) - \operatorname{tr}\big(\mathbf{C}_{\mathsf{S}}^H \mathbf{R}_{\mathsf{S}}^{-1} \mathbf{C}_{\mathsf{S}}\big).$$

Averaging over S proves (46). Retaining the mean-mismatch term and the completed-square term, subtracting the minimum conditional MSE, and averaging proves (47). Strict positivity of $\mathbf{R}_{\mathsf{S}}$ establishes uniqueness up to almost-sure equality.

Appendix F
Proof of Theorem 3

Apply Lemma 2 with $U = \mathsf{O} = (\boldsymbol{\theta}, \mathsf{S})$. Under A1–A2,

$$\boldsymbol{\mu}_{\mathsf{O}} = \boldsymbol{\mu}_y(\boldsymbol{\theta}), \qquad \mathbf{R}_{\mathsf{O}} = \mathbf{R}_y(\boldsymbol{\theta}), \qquad \mathbf{C}_{\mathsf{O}} = \mathbf{C}(\boldsymbol{\theta}).$$

Assumption A3 implies $\mathbf{R}_y(\boldsymbol{\theta}) \succ \mathbf{0}$ almost surely. The same square-completion argument as above gives

$$\mathbf{W}_{\mathrm{or}} = \mathbf{R}_y(\boldsymbol{\theta})^{-1} \mathbf{C}(\boldsymbol{\theta}), \qquad \mathbf{a}_{\mathrm{or}} = \boldsymbol{\mu}_b - \mathbf{W}_{\mathrm{or}}^H \boldsymbol{\mu}_y(\boldsymbol{\theta}).$$

The corresponding Schur-complement bound ensures a finite-second-moment estimate. Averaging the conditional minimum MSE gives (52).

Define the oracle residual $\mathbf{e}_{\mathrm{or}} = \mathbf{b} - \widehat{\mathbf{b}}_{\mathrm{or}}$. The affine normal equations give $\mathbb{E}[\mathbf{e}_{\mathrm{or}} \mid \boldsymbol{\theta}, \mathsf{S}] = \mathbf{0}$ and

$$\mathbb{E}\big[(\underline{\mathbf{y}} - \boldsymbol{\mu}_y(\boldsymbol{\theta}))\mathbf{e}_{\mathrm{or}}^H \mid \boldsymbol{\theta}, \mathsf{S}\big] = \mathbf{0}.$$

For fixed $(\boldsymbol{\theta}, \mathsf{S})$, the difference $\widehat{\mathbf{b}}_{\mathsf{S}}^\star - \widehat{\mathbf{b}}_{\mathrm{or}}$ is affine in $\underline{\mathbf{y}}$. The normal equations therefore imply

$$\mathbb{E}\Big[\mathbf{e}_{\mathrm{or}}^H (\widehat{\mathbf{b}}_{\mathsf{S}}^\star - \widehat{\mathbf{b}}_{\mathrm{or}})\Big] = 0.$$

Expanding

$$\mathbf{b} - \widehat{\mathbf{b}}_{\mathsf{S}}^\star = \mathbf{e}_{\mathrm{or}} + (\widehat{\mathbf{b}}_{\mathrm{or}} - \widehat{\mathbf{b}}_{\mathsf{S}}^\star)$$

and using this orthogonality gives

$$\mathcal{J}_{\mathsf{S}}^\star = \mathcal{J}_{\mathrm{or}}^\star + \mathbb{E}\Big[\|\widehat{\mathbf{b}}_{\mathsf{S}}^\star - \widehat{\mathbf{b}}_{\mathrm{or}}\|_2^2\Big].$$

This proves (53).

To establish orthogonality between the two estimator corrections, first decompose

$$\underline{\mathbf{y}} - \boldsymbol{\mu}_{\mathsf{S}} = (\underline{\mathbf{y}} - \boldsymbol{\mu}_y(\boldsymbol{\theta})) + (\boldsymbol{\mu}_y(\boldsymbol{\theta}) - \boldsymbol{\mu}_{\mathsf{S}}).$$

The first term is conditionally orthogonal to $\mathbf{e}_{\mathrm{or}}$ by the oracle normal equation. The second is $(\boldsymbol{\theta}, \mathsf{S})$-measurable, while the oracle residual has zero conditional mean given that information. Conditioning down to S therefore gives

$$\mathbb{E}\big[(\underline{\mathbf{y}} - \boldsymbol{\mu}_{\mathsf{S}})\mathbf{e}_{\mathrm{or}}^H \mid \mathsf{S}\big] = \mathbf{0}.$$

Likewise, the side-information-optimal residual $\mathbf{e}_{\mathsf{S}} = \mathbf{b} - \widehat{\mathbf{b}}_{\mathsf{S}}^\star$ satisfies

$$\mathbb{E}[(\underline{\mathbf{y}} - \boldsymbol{\mu}_{\mathsf{S}})\mathbf{e}_{\mathsf{S}}^H \mid \mathsf{S}] = \mathbf{0}.$$

Since $\widehat{\mathbf{b}}_{\mathsf{S}}^\star - \widehat{\mathbf{b}}_{\mathrm{or}} = \mathbf{e}_{\mathrm{or}} - \mathbf{e}_{\mathsf{S}}$, subtraction gives

$$\mathbb{E}\Big[(\underline{\mathbf{y}} - \boldsymbol{\mu}_{\mathsf{S}})(\widehat{\mathbf{b}}_{\mathsf{S}}^\star - \widehat{\mathbf{b}}_{\mathrm{or}})^H \mid \mathsf{S}\Big] = \mathbf{0}. \tag{73}$$

Both optimal estimates have conditional mean $\boldsymbol{\mu}_b$ given S: this holds directly for the S-optimal estimate and follows by the tower property for the oracle estimate. Their difference thus has zero conditional mean.

The plug-in correction can be written as

$$\begin{aligned} \widehat{\mathbf{b}}_{\mathrm{PI}} - \widehat{\mathbf{b}}_{\mathsf{S}}^\star &= \mathbf{d}_{\mathrm{PI}}(\mathsf{S}) \\ &\quad + (\mathbf{W}_{\mathrm{PI}} - \mathbf{W}_\star)^H (\underline{\mathbf{y}} - \boldsymbol{\mu}_{\mathsf{S}}), \end{aligned}$$

where

$$\begin{aligned} \mathbf{d}_{\mathrm{PI}}(\mathsf{S}) &= \mathbf{a}_{\mathrm{PI}} + \mathbf{W}_{\mathrm{PI}}^H \boldsymbol{\mu}_{\mathsf{S}} - \boldsymbol{\mu}_b \\ &= \mathbf{W}_{\mathrm{PI}}^H (\boldsymbol{\mu}_{\mathsf{S}} - \widehat{\boldsymbol{\mu}}_y). \end{aligned}$$

The constant term is orthogonal to the information correction because that correction has zero conditional mean. The centered-observation term is orthogonal by (73). Conditioning on S and then averaging proves (55). Here, as in the excess-risk identity, the plug-in receiver is assumed admissible, so these inner products are integrable.

Adding $\mathcal{G}_{\mathrm{PI}} = \mathcal{J}_{\mathrm{PI}} - \mathcal{J}_{\mathsf{S}}^\star$ and $\mathcal{G}_{\mathrm{info}} = \mathcal{J}_{\mathsf{S}}^\star - \mathcal{J}_{\mathrm{or}}^\star$ proves (54). The established orthogonality gives this decomposition its Pythagorean interpretation.

Finally, the explicit information-loss expression follows by writing

$$\begin{aligned} \widehat{\mathbf{b}}_{\mathsf{S}}^\star - \widehat{\mathbf{b}}_{\mathrm{or}} &= \mathbf{W}_\star^H (\boldsymbol{\mu}_y(\boldsymbol{\theta}) - \boldsymbol{\mu}_{\mathsf{S}}) \\ &\quad + (\mathbf{W}_\star - \mathbf{W}_{\mathrm{or}})^H (\underline{\mathbf{y}} - \boldsymbol{\mu}_y(\boldsymbol{\theta})). \end{aligned}$$

Conditioned on $(\boldsymbol{\theta}, \mathsf{S})$, the second term is centered and has covariance determined by $\mathbf{R}_y(\boldsymbol{\theta})$. The cross term therefore vanishes. Taking the squared norm and averaging gives (56).

APPENDIX G
PROOF OF COROLLARY 1

Equation (53) expresses $\mathcal{G}_{\mathrm{info}}$ as the expectation of the nonnegative random variable

$$\|\widehat{\mathbf{b}}^{\star}_{\mathsf{S}} - \widehat{\mathbf{b}}_{\mathrm{or}}\|_2^2.$$

Its expectation is zero if and only if it is zero almost surely, which is equivalent to equality of the two estimates almost surely.

APPENDIX H
PROOF OF THEOREM 4

Fix a state j with $\Pr(Z = j) > 0$. Because Z is a function of S, A1 and the tower property give

$$\mathbb{E}[\mathbf{b} \mid Z = j] = \boldsymbol{\mu}_b, \qquad \mathrm{Cov}(\mathbf{b} \mid Z = j) = \mathbf{R}_b.$$

The conditional affine-WL problem therefore has the form of Lemma 2, with moments $\boldsymbol{\mu}_j$, $\mathbf{R}_j$, and $\mathbf{C}_j$. Since $\mathbf{R}_j \succ \mathbf{0}$, square completion gives the unique coefficients in (58). Coefficients assigned to zero-probability states do not affect the MSE. The same Schur-complement argument used for the continuous receiver establishes admissibility.

Every Z-dependent receiver is also an S-dependent receiver. To obtain the exact finite-state penalty, set

$$\mathbf{d}_Z(\mathsf{S}) = \mathbf{a}^{\star}_Z + (\mathbf{W}^{\star}_Z)^H \boldsymbol{\mu}_{\mathsf{S}} - \boldsymbol{\mu}_b.$$

The difference between the optimal estimates is

$$\begin{aligned}\widehat{\mathbf{b}}^{\star}_Z - \widehat{\mathbf{b}}^{\star}_{\mathsf{S}} &= \mathbf{d}_Z(\mathsf{S}) \\ &\quad + (\mathbf{W}^{\star}_Z - \mathbf{W}_{\star})^H(\underline{\mathbf{y}} - \boldsymbol{\mu}_{\mathsf{S}}).\end{aligned}$$

Conditioned on S, the observation in the second term is centered. Hence,

$$\begin{aligned}&\mathbb{E}\Big[\|\widehat{\mathbf{b}}^{\star}_Z - \widehat{\mathbf{b}}^{\star}_{\mathsf{S}}\|_2^2 \mid \mathsf{S}\Big] \\ &\quad = \|\mathbf{d}_Z(\mathsf{S})\|_2^2 \\ &\qquad + \mathrm{tr}\big((\mathbf{W}^{\star}_Z - \mathbf{W}_{\star})^H \mathbf{R}_{\mathsf{S}} (\mathbf{W}^{\star}_Z - \mathbf{W}_{\star})\big).\end{aligned}$$

The right-hand side is exactly the conditional excess MSE in Theorem 2. Averaging proves (59).

The class inclusion also implies $\mathcal{J}^{\star}_{\mathsf{S}} \le \mathcal{J}^{\star}_{\mathcal{Q}}$ for every admissible quantizer $\mathcal{Q}$. Taking the infimum over $\mathfrak{Q}_Q(\boldsymbol{\psi})$ proves (61).

Finally, suppose $\boldsymbol{\psi}_1 = g(\boldsymbol{\psi}_2)$ almost surely. Any quantizer based on $\boldsymbol{\psi}_1$ can be implemented using $\boldsymbol{\psi}_2$ by first applying g. Thus, as classes of mappings from S to receiver states,

$$\mathfrak{Q}_Q(\boldsymbol{\psi}_1) \subseteq \mathfrak{Q}_Q(\boldsymbol{\psi}_2).$$

Taking the infimum over the larger class proves (62).

APPENDIX I
PROOF OF PROPOSITION 1

For a fixed codebook, assigning $\mathsf{S} = s$ to state j incurs conditional excess MSE $d(s; \mathbf{a}_j, \mathbf{W}_j)$. Consequently, the overall MSE is

$$\mathcal{J}^{\star}_{\mathsf{S}} + \mathbb{E}\big[d(\mathsf{S}; \mathbf{a}_{\mathcal{Q}(\mathsf{S})}, \mathbf{W}_{\mathcal{Q}(\mathsf{S})})\big].$$

The first term is independent of the assignment. For unrestricted routing, minimizing the distortion pointwise therefore gives (64). Because the codebook is finite, a measurable assignment can be obtained by selecting the smallest minimizing index whenever a tie occurs.

Conversely, for a fixed partition, the state probabilities and events $\{Z = j\}$ are fixed. The total MSE is the probability-weighted sum of the conditional MSEs in the occupied cells. Each codeword can therefore be optimized separately. For $\Pr(Z = j) > 0$, Theorem 4 gives

$$\mathbf{W}^{\star}_j = \mathbf{R}_j^{-1}\mathbf{C}_j, \qquad \mathbf{a}^{\star}_j = \boldsymbol{\mu}_b - (\mathbf{W}^{\star}_j)^H \boldsymbol{\mu}_j.$$

Zero-probability cells do not contribute to the objective.

Each assignment step and each codeword-update step thus minimizes the objective with the other component fixed. For admissible iterates with finite initial MSE, the resulting population MSE sequence is nonincreasing and bounded below by $\mathcal{J}^{\star}_{\mathsf{S}}$, so its objective values converge. This does not imply convergence to a globally optimal partition.